Microbiota stimulation generates LCMV-specific memory CD8+ T cells in SPF mice and determines their TCR repertoire during LCMV infection

Pedro Gonçalves, Sary El Daker, Florence Vasseur, Nicolas Serafini, Annick Lim, Orly Azogui, Helene Decaluwe, Delphine Guy-Grand, Antonio A. Freitas, James P. Di Santo, et al.

▶ **To cite this version:**

Pedro Gonçalves, Sary El Daker, Florence Vasseur, Nicolas Serafini, Annick Lim, et al.. Microbiota stimulation generates LCMV-specific memory CD8+ T cells in SPF mice and determines their TCR repertoire during LCMV infection. Molecular Immunology, 2020, 124, pp.125 - 141. 10.1016/j.molimm.2020.05.012 . hal-03490865

HAL Id: hal-03490865
https://hal.science/hal-03490865v1

Submitted on 22 Aug 2022

HAL is a multi-disciplinary open access archive for the deposit and dissemination of scientific research documents, whether they are published or not. The documents may come from teaching and research institutions in France or abroad, or from public or private research centers.

L'archive ouverte pluridisciplinaire **HAL**, est destinée au dépôt et à la diffusion de documents scientifiques de niveau recherche, publiés ou non, émanant des établissements d'enseignement et de recherche français ou étrangers, des laboratoires publics ou privés.

Distributed under a Creative Commons Attribution - NonCommercial 4.0 International License

Version of Record: https://www.sciencedirect.com/science/article/pii/S0161589020303539
Manuscript_c3ce41a6b86d73e777d9e18cc3d10b7e

Microbiota stimulation generates LCMV-specific memory CD8$^+$ T cells in SPF mice and determines their TCR repertoire during LCMV infection.

Pedro Gonçalves[1,2,3]*, Sary El Daker[1,6], Florence Vasseur[2], Nicolas Serafini[3,4], Annick Lim[4], Orly Azogui[2], Helene Decaluwe[1,7], Delphine Guy-Grand[4,5], Antonio A. Freitas[1], James P. Di Santo[3,4] & Benedita Rocha[1,2,#]

[1]Population Biology Unit, CNRS URA 196, Institut Pasteur, Paris, 75015; France
[2] INSERM, U1151, CNRS, UMR8253, Institut Necker Enfants Malades, Université Paris Descartes, Paris, 75015; France
[3]Innate Immunity Unit, INSERM, U668, Institut Pasteur, Paris, 75015; France
[4]INSERM U1223, Paris, 75015; France
[5]Lymphopoiesis Unit, INSERM U668, University Paris Diderot, Sorbonne Paris Cité, Cellule Pasteur, Institut Pasteur, Paris, 75015, France
[6]current address: KwaZulu-Natal Research Institute for TB and HIV (K-RITH), 4001; Durban, South Africa
[7]current address: Cytokines and Adaptive Immunity Laboratory, CHU Sainte-Justine Research Center; Department of Microbiology and Immunology, Faculty of Medicine, University of Montreal, Montreal; Immunology and Rheumatology Division, Department of Pediatrics, Faculty of Medicine, University of Montreal, Montreal, Quebec, Canada.

***Corresponding author**: P. Gonçalves, Institut Pasteur, 25 Rue du Dr. Roux, 75015 Paris, France; tel: +33601080704; e-mail: pedroffg@gmail.com; ORCID: 0000-0002-4127-1152

#Lead Contact: B. Rocha, Institut Pasteur, 25 Rue du Dr. Roux, 75015 Paris, France; tel: +33145688582;; e-mail: benedita.rocha@inserm.fr

© 2020 published by Elsevier. This manuscript is made available under the CC BY NC user license
https://creativecommons.org/licenses/by-nc/4.0/

Abstract

Both mouse and human harbour memory phenotype $CD8^+$ T cells specific for antigens in hosts that have not been previously exposed to these antigens. The origin and the nature of the stimuli responsible for generation of $CD44^{hi}$ $CD8^+$ T cells in specific pathogen-free (SPF) mice remain controversial. It is known that microbiota plays a crucial role in the prevention and resolution of systemic infections by influencing myelopoiesis, regulating dendritic cells, inflammasome activation and promoting the production of type I and II interferons. By contrast, here we suggest that microbiota has a direct effect on generation of memory phenotype $CD44^{hi}GP33^+CD8^+$ T cells. In SPF mice, it generates a novel $GP33^+CD44^{hi}CD8^+$ T cell sub-population associating the properties of innate and genuine memory cells. These cells are highly enriched in the bone marrow, proliferate rapidly and express immediate effector functions. They dominate the response to LCMV and express particular TCRβ chains. The sequence of these selected TCRβ chains overlaps with that of $GP33^+CD8^+$ T cells directly selected by microbiota in the gut epithelium of SPF mice, demonstrating a common selection mechanism in gut and peripheral $CD8^+$ T cell pool. Therefore microbiota has a direct role in priming T cell immunity in SPF mice and in the selection of TCRβ repertoires during systemic infection. We identify a mechanism that primes T cell immunity in SPF mice and may have a major role in colonization resistance and protection from infection.

Keywords: TCR repertoires; microbiota; innate memory $CD8^+$ T cells; bone marrow; LCMV

Abbreviations: BM - bone marrow; GF - germ-free; HP - homeostatic proliferation; LCMV - Lymphocytic choriomeningitis virus; LN - lymph nodes; NKR - natural killer receptors; SP - spleen; SPF - specific pathogen free; TCR - T cell receptor; TLR4 - Toll-like receptor; T_{VM} - virtual memory T cells; T_{RM} - tissue resident memory cells

1. Introduction

Both mouse and human harbour memory phenotype $CD8^+$ T cells specific for antigens in hosts that have not been previously exposed to these antigens. In mice, memory phenotype ($CD44^{hi}$) $CD8^+$ T cells are present in specific pathogen free (SPF) and even in germ-free (GF) mice (Haluszczak et al., 2009; Lee et al., 2013). Some researchers classified these cells as virtual memory $CD8^+$ T (T_{VM}) and propose that they were generated in a TCR-independent manner (Haluszczak et al., 2009; White et al., 2016). The majority of $CD44^{hi}$ $CD8^+$ T cells are believed to be generated by homeostatic proliferation (HP) in the perinatal period. When the first mature thymocytes (putatively considered naïve cells) leave the thymus to colonize the "empty" peripheral T cell pool, a fraction is recruited to undergo HP reconstituting the $CD44^{hi}CD8^+$ T cell compartment (reviewed in (Freitas and Rocha, 2000)). In adult mice, these $CD44^{hi}$ $CD8^+$ T cells are highly functional, exhibiting more rapid proliferation and cytokine production after TCR stimulation compared to true naïve $CD44^-CD8^+$ T cells (Duffy et al., 2012; Haluszczak et al., 2009; Lee et al., 2013; Raue et al., 2013), but the role of these cells during immune responses remain controversial. Recently a elegant study showed that early-life derived $CD8^+$ T cells preferentially become HP $CD44^{hi}CD8^+$ T cells in adult SPF mice (Smith et al., 2018). These early-life derived $CD44^{hi}CD8^+$ T cells exhibits rapid and innate-like functions in response to cytokine signals, expressed higher levels of CXCR3 and effector proteins IFN-γ and granzyme B. In contrast, the adult derived $CD8^+$ T cells predominantly give rise to naïve $CD44^-CD8^+$ T cells with slower kinetics (Smith et al., 2018). The adoptive co-transfer of congenically labeled TCR transgenic $CD8^+$ T cells showed that early-life derived $CD44^{hi}CD8^+$ T cells are the first $CD8^+$ T cells to respond to *Listeria monocytogenes* infection in adult mice (Smith et al., 2018). However, there was a substantial accumulation of memory $CD8^+$ T cells with age, consistent with cumulative antigen exposure over the mice (Quinn et al., 2018) and human (Su et al., 2013) life span, suggesting that HP

CD44^{hi} CD8^{+} T cell heterogeneity was underestimated in previous studies. The protective potential of CD44^{hi}CD8^{+} T cells was also mostly tested in model infections with TCR transgenic CD8^{+} T cells (Smith et al., 2018). In addition, CD44^{hi}CD8^{+} T cells are particularly abundant in the bone marrow (BM) of unmanipulated SPF mice (Goncalves et al., 2017), the role of these polyclonal host CD44^{hi}CD8^{+} T cells during primary immune responses and their TCR repertoire remain unknown.

The origin and the nature of the stimuli responsible for HP of CD44^{hi} CD8^{+} T cells remain also controversial. Cytokine stimulation was claimed to generate HP CD44^{hi} CD8^{+} (Haluszczak et al., 2009; White et al., 2016), but other studies have shown that cytokines are necessary but not sufficient for HP (Freitas and Rocha, 2000). Besides cytokine stimulation, HP required TCR stimulation, the extent of HP being proportional to the extent of TCR cross-reactivity (Hao et al., 2006). HP was attributed to the recognition of cross-reactive self-antigens (Quinn et al., 2016; Surh and Sprent, 2000), since the OVA-specific CD44^{hi}CD8^{+} population in the spleen (SP) was not modified in germ-free (GF) conditions, and HP was maintained after microbiota elimination by antibiotic treatment (Haluszczak et al., 2009; Kawabe et al., 2017; Quinn et al., 2016). However, although antibiotics killed resident bacteria, they could not ensure that all bacteria components were eliminated. Other experiments supported a major role of microbiota in the generation of HP CD44^{hi} CD8^{+} (Beura et al., 2016; Feng et al., 2010; Kieper et al., 2005). Thus, when polyclonal CD4^{+} T cells where adoptively transferred to severe combined immunodeficiency (SCID) germ-free (GF) mice they homeostatic proliferated slowly, while when transferred to SCID SPF mice they proliferated vigorously (Feng et al., 2010; Kieper et al., 2005). Also, the number of CD44^{hi}CD8^{+} T cells is much reduced in GF mice (Beura et al., 2016). Using different animals models studies showed that microbiota-derived antigens generate CD44^{hi}CD8^{+} T cells in part mediated by sustained TCR stimulation (Mani et al., 2019; Tanoue et al., 2019). Immediately

after birth, newborn mice experience rapid colonization by microbiota that participate in the development of their immune system and possible in generation of early-life derived HP $CD44^{hi}CD8^{+}$ T cells (Smith et al., 2018). The existence of different types of $CD8^{+}$ T cells cross-reactive with self-antigens (Quinn et al., 2016; Surh and Sprent, 2000) or microbiota-antigens (Feng et al., 2010; Kieper et al., 2005; Mani et al., 2019; Tanoue et al., 2019) could explain the contradictory conclusions in the stimuli responsible for HP $CD44^{hi}$ $CD8^{+}$ T cells (White et al., 2017). Addressing the role of microbiota in generation of HP $CD44^{hi}CD8^{+}$ T cells is an important issue since microbiota is known to have a major protective effect against systemic infections (Becattini et al., 2017).

We recently quantified precisely the number, organ distribution and the TCRβ (TRBV) repertoire of $CD8^{+}$ T cells specific for the GP33 peptide of the LCMV ($GP33^{+}$ cells) in all lymphoid organs of SPF B6 mice. Surprisingly, we found that the majority of $GP33^{+}$ cells were not naïve, but rather expressed CD44, and were particularly abundant in the BM (Goncalves et al., 2017). Here, we study their phenotypic characteristics and directly track the effector $GP33^{+}$ cells numbers through the course of LCMV infection, together with clonotypic TCR repertoire analysis. We here showed that $CD44^{hi}$ $GP33^{+}$ T cells accumulate adaptive and innate functions. $CD44^{hi}$ $GP33^{+}$ T cells are preferentially selected during LCMV infection. This study is the first to our knowledge to demonstrate by TCR repertoire analyses that these cells are preferentially selected during LCMV infection. Our results suggest also that microbiota stimulation generates these cells in SPF mice. Their TCRβ repertoire is conditioned by microbiota stimulation. In conclusion, these data suggest that microbiota stimulates antigen-specific $CD8^{+}$ T cells, and selects their TCR repertoire during primary infection. These data reveal a new major mechanism conditioning the effective responses to infection in mice harbouring a normal microbiota.

2. Materials and methods

2.1. Mice and immunization protocols

C57BL/6 (B6) specific-pathogen-free (SPF-1 and SPF-2) or germ-free (GF) mice were obtained from the breeding colonies of the Pasteur Institute. CD45.1^{+} Rag2$^{-/-}$ B6 mice expressing a transgenic TCR specific for LCMV epitope GP_{33-41} (GP33^{+}) P14 (P14) were obtained from our breeding colonies at the Centre de Distribution, Typage et Archivage (CDTA, Orleans, France). For LCMV infection, mice were injected i.p. with 2.5x10^{5} PFU of LCMV Armstrong. Mice were kept in isolators until sacrifice.

2.2. Quantification and characterization of antigen-specific CD8^{+} T cells

The method to the evaluation of the number of antigen-specific cells in spleen (SP) and the bone marrow (BM) was described in detail previously (Goncalves et al., 2017; Sung et al., 2013), multiple steps being used to optimize cell recovery and quantify cell loss during the preparation steps. The total number of BM cells was obtained by multiplying the number of cells recovered from two femurs by 7.9, as previously described (Slifka et al., 1995). Intraepithelial lymphocytes (IELs) of the murine small intestine were recovered as we described previously (Guy-Grand et al., 2013). Briefly, cell suspensions were depleted from non-CD8^{+} T cells followed by staining with APC or PE-labeled H-2D^{b} or H-2K^{d} dextramers loaded with different peptides (Dextramers®, Immudex, Copenhagen, Denmark) (Goncalves et al., 2017; Sung et al., 2013). This was followed by the incubation at 4°C during 30 min with multiple MoAbs obtained from BD Pharmingen (San Diego, CA, USA): anti-CD45.1 (A20), anti-CD3ε (145-2C11), anti-CD8β (H35-172), anti-CD44 (1M781), anti-CD62L (MEL-14), anti-CD5 (Ly-1), anti-CD122 (TM-B1), anti-CD25 (PC61), anti-PD-1 (29F.1A12), anti-KLRG1 (2F1), anti-CD69 (H1.2F3), anti-CD103 (M290), anti-CD49b (DX5), anti-CD160 (ebioCNIX46-3), anti-CD107a (1D4B), anti-TLR4/MD-2 (MTS510), anti-ASGM1,

anti-NKG2D (1D11), anti-CD183 (CXCR3-173), anti-Vβ13 (F23.1), anti-Vβ29 (TR310), anti-IFN-γ (XM61.2), anti-GranzB (6B11). Dead cells were excluded by Sytox Green dead cell stain (Thermo Fisher Scientific, MA USA). Labelled populations were diluted in 0.5 ml of FACS flow buffer and acquired using the low-speed mode in a FACSCanto II or in a FACS LSRFortessa flow cytometer (Becton Dickinson, Franklin Lakes, NJ, USA). Different single cell $CD8^+$ populations were sorted (FACS-Aria II system, Becton Dickinson, Franklin Lakes, NJ, USA) into 96-well PCR plates (purity ≥ 99%). The data analysis was performed using FlowJo software (TreeStar, Ashland, OR).

2.3. Single-cell cDNA synthesis, nexted RT-PCR and sequencing

Analysis of TRBV usage was carried out by a single-cell multiplex RT-PCR developed in our laboratory, followed by the direct sequencing of the PCR products was described in detail previously (Goncalves et al., 2017).

2.4. Microbial DNA extraction, 16S rRNA sequencing and analysis

Fresh mouse stool samples were also collected and were immediately stored at -80 °C until DNA extraction was performed. Total fecal DNA was extracted using the NucleoSpin® Soil kit (MACHEREY-NAGEL®) following the protocol using both physical and chemical lysis. DNA concentrations were determined using Nanodrop spectrophotometer (Thermo Scientific). The V3-V4 region of the bacterial 16S rDNA region were PCR amplified with V3-340F (CCTACGGRAGGCAGCAG) and V4-805R (GGACTACHVGGGTWTCTAAT) barcoded primers. PCR products were cleaned using Ampure magnetic purification beads (Agencourt AMPure XP Kit), quantified with the QuantiFluor® ONE dsDNA kit (Promega), and pooled in equal amounts of each PCR product. Library pools were loaded at 12pM with a 15% PhiX spike for diversity and sequencing control, onto a v3 300-bp paired end reads

cartridge for sequencing on the Illumina MiSeq NGS platform. After removing reads containing incorrect primer or barcode sequences and sequences with more than one ambiguous base, we recovered from 16 samples a total of 2.467.335 reads (83% mapped, 108.388 mapped reads on average). The bioinformatics analysis was performed as previously described (Quereda et al., 2016). Briefly, amplicons were clustered into operational taxonomic units (OTU) with VSEARCH (v1.4) and aligned against the SILVA database. The clustering was performed at 98% sequence identity threshold, producing 386 OTUs. The input amplicons were then mapped against the OTU set to get an OTU-abundance table containing the number of reads associated with each OTU. The normalization, statistical analyzes and multiple visualization were performed with SHAMAN (SHiny application for Metagenomic Analysis (shaman.c3bi.pasteur.fr) based on R software.

2.5. In vitro cytokine stimulation assay

Bulk $CD44^{-}$ and $CD44^{hi}$ populations were sorted to purity ≥ 99%, and $5x10^5$ sorted cells plated on 12-wells plates in RPMI medium supplemented with 2% foetal calf serum. They were cultured overnight (18h) with medium supplemented with various cytokines: IL-12 (10 ng/ml), IL-18 (10 ng/ml), IL-2 (10 ng/ml) and IL-15 (10 ng/ml) (R&D). For intracellular cytokines staining, cells were incubated in the presence of GolgiPlug™ (Brefeldin A solution, BD) for 4 h at 37°C, fixed, permeabilized, and stained by Cytofix/Cytoperm Kit (BD Biosciences, San Jose, CA) according to the manufacturer's instructions, followed by the evaluation of the intra-cytoplasmatic expression of IFN-γ or Granzyme B. Samples were acquired on LSRFortessa (BD) and barriers identifying positive cells were established in the same populations, labelled with isotype controls.

2.6. Identification of in vivo dividing cells

Bromodeoxy Uridine (BrdU) was purchased from Sigma, (St. Louis, MO). Mice at day 3 and 5 post LCMV infections were injected i.p. with 1 mg BrdU. BrdU incorporation was studied in different organs one hour after injection using the Cytofix/Cytoperm kit (BD Biosciences, San Jose, CA) according to the manufacturer's instructions.

2.7. Bioinformatic determination of cross-reactivity with self-antigens

We used the iCrossR webserver, which performs assessment of cross-reactivity (CR) indices in different tissues (Jaravine et al., 2017).

2.8. Statistical analysis

Statistics were performed using Prism 5, GraphPad software (San Diego, USA). Statistical significance of the difference between two groups was evaluated by the Mann-Whitney U test. Single continuous variable data were analyzed by Kruskal-Wallis (KW) followed by Dunn's Multiple Comparison Test. For all these tests, a cut-off value of $p \leq 0.05$ was chosen (*$p \leq 0.05$; **$p \leq 0.01$; ***$p \leq 0.001$).

3. Results

3.1. Similarities and differences between $CD44^{hi}GP33^{+}$ cells and virtual memory $CD8^{+}$ T cells.

3.1.1. $CD44^{hi}GP33^{+}$ cells have characteristics of antigen-experienced memory $CD8^{+}$ T cells.

The presence of $CD44^{hi}$ $CD8^{+}$ T cells with different antigen specificities was already described in SPF mice (Haluszczak et al., 2009; Lee et al., 2013). We studied different LCMV epitopes (NP376, GP33, GP276 and GP34) and we found $CD44^{hi}$ $CD8^{+}$ T cells specific for all

of these antigens, particularly abundant in the BM of SPF B6 mice (not shown) (Goncalves et al., 2017). Therefore, we studied the LCMV immune-dominant $GP33^+$ cells and an unrelated non-self non-microbial-associated antigen, ovalbumin (OVA) in the following experiences. First, we compare the phenotypic features of antigen-specific $CD44^{hi}GP33^+$ and $CD44^-GP33^+$ cells of naïve SPF-1 B6 mice (Figure 1). The method to identify antigen-specific $CD8^+$ cells was described in detail previously (Sung et al., 2013) (Supplementary Figure 1, Supplementary Note 1). Analysis of the $CD44^{hi}GP33^+$ compound phenotype showed they correspond to a $CD8^+$ T cell subtype, different from previously described virtual memory T cells (T_{VM}) (Haluszczak et al., 2009; White et al., 2016) or tissue resident memory cells (T_{RM}). While T_{VM} have a $CD49d^{low}CD62L^+CD25^{low}CD69^{low}CD103^{low}$ phenotype (Haluszczak et al., 2009), $CD44^{hi}GP33^+$ were $CD49d^{hi}$ and comprised both $CD62L^+$ and $CD62L^-$ cells (Figure 1A). A fraction expressed the early activation markers CD25 and CD69 (Figure 1B) and the epithelial cell-binding integrin αEβ7 (CD103) (not shown), expressed by $T_{RM,}$ but lack killer cell lectin receptor G1 (KLRG1) (Figure 1C) (Tanoue et al., 2019). Interestingly, about half of total bone marrow (BM) $CD8^+$ $CD44^{hi}$ cells express also CD69 and the double labelling with CD69 and CD103 showed that these markers were co-expressed in 32% of the same cells (Figure 1D). Besides, $CD44^{hi}GP33^+$ cells were $CCR7^+PD\text{-}1^{low}$ (Figure 1E), while T_{RM} are $CD62L^-CCR7^-PD1^{hi}$ (Debes et al., 2005). In addition, T_{RM} cells have reduced expression levels of CD122, CD27, and Ly6C and $CD44^{hi}GP33^+$ cells express these markers at higher levels (not shown).

Not all $CD44^{hi}$ $CD8^+$ T cells from SPF mice expressed the above markers. More than 90% of the total $CD44^{hi}$ cells were $CD49d^{low}$ (Quinn et al., 2018) and express higher levels of CD5 and CD122 comparatively to $CD44^{hi}GP33^+$ cells (results not shown), features of T_{VM} cells (Drobek et al., 2018; Haluszczak et al., 2009). For example, $CD44^{hi}OVA^+$ cells have the phenotype of T_{VM} $CD49d^{low}CD62L^+$ (Supplementary Fig. 2). These results suggest that

$CD44^{hi}CD8^{+}$ T cell pool present in SPF mice is a heterogeneous population of T_{VM} and other phenotypic $CD44^{hi}$ $CD8^{+}$ T cells.

3.1.2. $CD44^{hi}GP33^{+}$ cells are preprogrammed to mount a rapid innate-like effector response.

Analysis of $CD44^{hi}GP33^{+}$ showed they expressed multiple characteristics of innate lymphocytes (Seyda et al., 2016). Although lacking CD161 (NK1.1) (not shown) they expressed very high levels of several natural killer receptors (NKR). As compared to $CD44^{-}$ $GP33^{+}$ T cells, the % of cells expressing NKG2D and ASGM1 as well as its expression level was much increased (Figure 2A, B). As innate lymphoid cells (Seyda et al., 2016) a fraction up-regulated the expression of multiple receptors associated with effector functions: CD11a and CD11b, CD160 and CD107a (Figure 2A, B). They also expressed multiple receptors allowing a TCR-independent stimulation. Besides, $CD44^{hi}GP33^{+}$ expressed ASGM1 and a fraction also expresses TLR4 (CD284) (Huggins et al., 2019; Loser et al., 2010) (Figure 2A, B), receptor for flagellin and LPS respectively. They express higher levels of CXCR3 (Figure 3A, B), that defines a subset of innate cells that can be activated to mediate effector functions in the absence of TCR stimulation (Smith et al., 2018; Soudja et al., 2012). They up-regulated the expression of multiple cytokine receptors, CD121a (IL-1βR), CD218a (IL-18R) and CD122 (IL2βR, IL-15R) (Figure 3A, B), allowing them to receive inflammasome and IL-15 signals. After overnight incubation with a cocktail of cytokines previously used (Haluszczak et al., 2009), $CD44^{hi}GP33^{+}$ increase in numbers (Figure 3C) and mediated effector functions (Figure 3D, E), whereas naïve $CD44^{-}GP33^{+}$ T cells failed to respond. We conclude that by their compound phenotype and TCR-independent effector functions the $CD44^{hi}GP33^{+}$ cells from SPF mice differ from "conventional" memory $CD8^{+}$ T cells (White et al., 2017). These results suggest that $CD44^{hi}GP33^{+}$ can provide protection against infections even in the absence of cognate antigen exposition.

3.2. The role of CD44^{hi}GP33^{+} CD8^{+} T cells during primary immune responses.

We observe that overnight incubation with GP33 peptide pulsed antigen presenting cells (APC) promote CD44^{hi}GP33^{+} increase in numbers (not shown) and induction of effector functions. More than 90% of CD44^{hi}GP33^{+} cells express CD69 (marker for early activation) and produce IFN-γ (Supplementary Fig. 3). CD44^{hi}GP33^{+} cells express more CD69 and IFN-γ than naïve CD44^{-}GP33^{+} cells activated in the same conditions, suggesting a fast TCR-dependent induced activation and strong effector functions as demonstrated for other CD44^{hi} antigen-specific cells (Duffy et al., 2012; Haluszczak et al., 2009; Lee et al., 2013; Raue et al., 2013).

3.2.1. CD44^{hi}GP33^{+} cells are preprogrammed to mount a rapid early effector response.

To evaluate the role of CD44^{hi}GP33^{+} T cells during systemic infection we first studied their accumulation kinetics and division rates after *in vivo* infection of SPF mice with LCMV (Figure 4A; Supplementary Fig. 4). The kinetics of the primary immune response of GP33^{+} cells in the SP and LN of SPF mice (Supplementary Fig. 4) was as described previously (Murali-Krishna et al., 1998). By day 4 after priming the number GP33^{+} cells was not significantly increased. This was expected since naïve T cells have a long-lag time before division (Veiga-Fernandes et al., 2000). Responses peaked at day 7, followed by a contraction phase where most cells disappeared, and generate the memory pool.

The responses in the BM were very different. CD44^{hi}GP33^{+} T cells were particularly abundant in the BM of SPF mice (Figure 4B) (Goncalves et al., 2017), a key site for priming of T cells specific for blood-borne antigens (Duffy et al., 2012; Feuerer et al., 2003). Interestingly, the number of GP33^{+} cells was already 7 fold increased by day 4 after infection (Figure 4C). These results indicated a precocious activation and division of GP33^{+} cells in the BM, a behaviour characteristic of memory cells (Veiga-Fernandes et al., 2000). Responses

also peaked at day 7, but the contraction phase was virtually absent (Supplementary Fig. 4B). We conclude that after LCMV infection, $GP33^+$ cells in the SP and LN behaved as expected from naïve cells in a primary immune response, while $GP33^+$ cells in the BM behaved as we previously described in conventional memory cells (Veiga-Fernandes et al., 2000).

To confirm these different behaviours, we determined the % of $GP33^+$ cells in the S phase of the cell cycle after a single pulse of BrdU (Figure 4D, E). In the SP and LN 31-42% of $GP33^+$ cells were $BrdU^+$ by day 3 after priming. The percentage of $BrdU^+$ cells in the SP declined to an average of 20% at day 5, when $GP33^+$ cells approached the response peak. By contrast in BM, an average of 66% of $GP33^+$ cells were in S phase at day 3, and yet 42% were cycling at day 5 after immunization. Less than 5% of $CD44^{hi}GP33^-CD8^+$ T cells were $BrdU^+$ in SP and LN, where almost 20% were cycling in BM at day 3 or 5 after priming, suggesting also a preferential proliferation of other antigen specificities (e.g. NP376, GP276) in BM.

These results confirm that $GP33^+$ cells located in the BM have a very different behaviour from those located in the SP and LN. They show an earlier activation, a much increased and persistent proliferation rates and increased survival. The different behaviour of $GP33^+$ cells located in the BM indicates an important advantage of $CD44^{hi}GP33^+$ in the primary immune response to LCMV infection.

3.2.2. $CD44^{hi}GP33^+CD8^+$ T cells can trafficking from bone marrow to the periphery.

A number of reports have indicated that BM is a major reservoir for recirculating $CD44^{hi}CD8^+$ T cells (Klonowski et al., 2004; Stark et al., 2018; Thomas et al., 2011). Some other suggest that BM resident $CD44^{hi}CD8^+$ T might be tissue resident memory cells (T_{RM}) (Pascutti et al., 2019). $CD44^{hi}GP33^+$ cells show an earlier activation and much increased proliferation rates in BM, therefore we considered the possibility of migration of these cells to the periphery. Because TCRβ (TRBV) repertoires of $GP33^+$ cells were essentially unique to

each individual mouse ("private") and diverse (Goncalves et al., 2017), if this is the case, the TRBV repertoire in the periphery should significantly overlap with that in BM. We sorted $CD44^{hi}GP33^{+}$ cells from BM, SP and LNs at different time points after LCMV infection and we analyzed their clonotypic TRBV repertoires (Goncalves et al., 2017). In total, we analyzed over 2,026 GP33-specific $CD8^{+}$ $\alpha\beta^{+}$ T cells at the single-cell level in all mice at different time points after LCMV infection. The sequences are shown in Supplementary Table 1. In the main text we show the modifications of the percentage of cells expressing different TRBV genes and the compound composition of all CDR3 regions. Interestingly, effector $GP33^{+}$ $CD8^{+}$ T cell clonotypes at day 7 post-infection are widely dispersed between different organs (Table 1, Supplementary Table 1), single-cell TRBV sequences that were prominent BM are also present in SP and LN, suggesting that T cell trafficking from and to BM might be precocious in early effector phase. These results suggest that after the early activation and proliferation in BM, effector $GP33^{+}$ cells were able to migrate to the infected organs and contribute to LCMV clearance.

3.2.3. The TRBV repertoire of $GP33^{+}$ cells during LCMV infection converges to that of $CD44^{hi}GP33^{+}$ cells already present in SPF mice.

We next evaluated the relative contribution of $CD44^{-}$ and $CD44^{hi}GP33^{+}$ cells to the immune response to LCMV infection. Since after *in vivo* infection naïve $CD44^{-}GP33^{+}$ become activated expressing $CD44^{hi}$, CD44 expression levels could no longer discriminate $GP33^{+}$ cells of naïve versus $CD44^{hi}$ origin. However, we described that $CD44^{-}GP33^{+}$ T cells had a biased TCRB repertoire, different from that of $CD44^{hi}GP33^{+}$ cells (Goncalves et al., 2017). The major differences between naïve and $CD44^{hi}$ $GP33^{+}$ cells were found in the expression frequencies of TRBV13 genes (coding for the Vβ8 proteins) and TRBV29 gene (coding for the Vβ7 protein). Up to 40-47% of $CD44^{-}GP33^{+}$ cells expressed TRBV13/Vβ8, in

contrast to a 15-20% frequency in the $CD44^{hi}GP33^{+}$ repertoires. By contrast, only 4% of $CD44^{-}GP33^{+}$ expressed the TRBV29/Vβ7 chain while an averaged 12% of $CD44^{hi}GP33^{+}$ cells expressed this TRBV (Figure 5A, B). Other TRBV genes showed but minor differences (Supplementary Table 1).

Next we evaluated how $GP33^{+}$ TRBV repertoires were modulated during LCMV infection (Figure 5C, Supplementary Table 1). As striking differences we found a major and progressive decline in the frequency of cells expressing TRBV13, concomitant with a major and progressive selection of TRBV29 expressing cells. Overall, the frequency of $TRBV13^{+}$ cells dropped from 47% of $CD44^{-}GP33^{+}$ naïve cells to an average of 12% of secondary effectors (Figure 5C). $TRBV29^{+}$ cells followed the opposite trend. This TRBV, which was more abundant in the $CD44^{hi}GP33^{+}$ in SPF mice, was further enriched in the effector phase, persisted in similar frequencies in the memory compartment, and was further increased in secondary immune responses (Figure 5C). While in SPF mice TRBV29 was expressed by ≈ 12% of $CD44^{hi}GP33^{+}$ $CD8^{+}$ T cells, ≈ 38% of $GP33^{+}$ effectors cells expressed TRBV29 in a secondary immune response (Figure 5C). Of note, this modulation of the TRBV repertoire was similar in each animal, and common to all organs (Table 1, Supplementary Table 1). These results suggest that TCR repertoire of $GP33^{+}$ cells during LCMV response shifts from that of naïve $CD44^{-}GP33^{+}$ (where $TRBV13/V\beta8^{+}$ cells predominate) to those expressing $TRBV29/V\beta7^{+}$. The preferential selection of TRBV29/Vβ7 repertoire is compatible with a major advantage of $CD44^{hi}GP33^{+}$ in the primary immune response to LCMV infection.

3.2.4. The role of TCR complementary-determining regions (CDRs) in selection of $GP33^{+}$ cells after LCMV infection.

In general, it is assumed that the CDR1 and CDR2 loops of the TCRβ interact with the α2 and α1 helix of MHC class I, while the highly diverse CDR3 loops are mainly responsible

for peptide recognition and repertoire selection (Das et al., 2015). Interestingly, we found a enrichment in asparagine (N) in CDR3 of TRBV29^{+} cells. This amino acid was already overexpressed by TRBV29^{+} primary effectors and was always dominant in position 7 in memory and secondary effectors (Supplementary Fig. 5A-E). These data suggest that the selection of TRBV29^{+} cells during LCMV responses had features of a type 2 immune response (Turner et al., 2006). In type 2 responses antigen binds to the CDR1 and CDR2 domains (encoded within the TCR germline variable sequence) of TRBV(29) gene, having conserved amino acids or "motifs" in the CDR3 (CASSxxxNxxEQYF) important to peptide recognition (Das et al., 2015) and involved in the selection of GP33^{+} cells during LCMV response (Adams et al., 2016; Cole et al., 2009). Besides asparagine, glycines (coded by the germ line TRBD genes) were present at higher frequency, but this occurred in both TRBV29^{+} and TRBV29^{-} cells. The higher expression of glycines was maintained throughout the response (Supplementary Fig. 5A-E). A CDR3 region enriched in glycines increases the flexibility of the TCR reported to lead to greater promiscuity in antigen recognition (Chowell et al., 2015; Stadinski et al., 2016) and increases TCR cross-reactivity (Birnbaum et al., 2014).

3.3. Nature of the stimuli responsible for generation of CD44^{hi}GP33^{+} CD8^{+} T cells.

3.3.1. GP33 and OVA peptide molecular mimicry.

To determine which type of cross-reactive antigens were responsible for the generation of different sub-populations of CD44^{hi}GP33^{+} CD8^{+} T cells we first performed an *in silico* search of molecular mimicry between GP33 and OVA peptides with self or microbiota-components. The BLAST search revealed that OVA peptide align 100% to multiple self components (Ge et al., 2004) and showed molecular mimicking with self-antigens present in different tissues (Supplementary Fig. 6A, B). OVA peptide showed also

molecular mimicking with microbiota components that besides are poorly represented within the microbiota (Supplementary Table 2). On the other hand, GP33 peptide showed low molecular mimicking with self-antigens (Supplementary Fig. 6A, B) (Quinn et al., 2016). However, the *in silico* search revealed that GP33 peptide showed molecular mimicking with multiple components present in bacterial strains (Supplementary Table 2). Bacterial strains predicted to have molecular mimicking with GP33 peptide represent ≈ 4% of the total mice fecal microbiota (*Clostridium*, *Staphylococcus* and *Peptococcus* genus) of SPF-1 mice determined by 16S ribosomal RNA (rRNA) sequencing (Supplementary Fig. 6H). These results suggest that $CD44^{hi}GP33^{+}$ cells and $CD44^{hi}OVA^{+}$ cells could be generated by cross-reactivity with different antigens. $CD44^{hi}GP33^{+}$ cells may be mostly generated by cross-reactivity with microbiota components present in gut of SPF mice.

3.3.2. Microbiota stimulation generates $CD44^{hi}GP33^{+}$ $CD8^{+}$ T cells.

Given the immense antigenic load present in microbiota, we hypothesized that some microbiota mimotopes can be responsible for the generation of $CD44^{hi}GP33^{+}$ cells in gut-associated lymphoid tissue (GALT) (Esterhazy et al., 2019; Harkiolaki et al., 2009; Li et al., 2019; Mani et al., 2019; Su et al., 2013; Tanoue et al., 2019; Yang et al., 2014). Activated $CD8^{+}$ T cells in GALT can migrate through the thoracic ducts to the blood vasculature, disseminating to peripheral lymphoid organs (Beura et al., 2018; Tanoue et al., 2019; Teng et al., 2016). In addition, microbiota mimotopes were shown to disseminate across the body and thus may stimulate recirculating $CD8^{+}$ T cells located elsewhere (Beura et al., 2018; Tanoue et al., 2019; Teng et al., 2016). To test this hypothesis we evaluated if the absence of microbiota under GF conditions decrease $CD44^{hi}GP33^{+}$ numbers in peripheral lymphoid organs. The total number of $CD8^{+}$ T cells (in SP and BM) is not significant different between GF and SPF-1 B6 mice (not shown), suggesting that GF mice have a normal T cell poiesis

(Khosravi et al., 2014). However, the GF condition induced an overall reduction of $CD44^{hi}CD8^{+}$ cells (Figure 6A) and the % and total number of $CD44^{hi}GP33^{+}$ was much reduced in the BM (Figure 6B, C). The total number of $CD44^{hi}GP33^{+}$ was reduced 80% in BM of GF mice. In accordance with the rare cross reactivity of OVA specific cells with microbiota components, we confirmed that the GF condition did not affect the number of $CD44^{hi}OVA^{+}$ cells in the SP (not shown), as reported previously (Haluszczak et al., 2009). In GF mice the phenotype of $CD44^{hi}GP33^{+}$ cells was also modified. In particular, almost all total $CD44^{hi}CD8^{+}$ and $CD44^{hi}GP33^{+}$ cells that that remain in GF condition were $CD49d^{low}$ (T_{VM}) (Figure 6D, E) (Drobek et al., 2018; Haluszczak et al., 2009). Interestingly, 92% of $CD44^{hi}CD8^{+}$ in the BM failed to express CD69 (Figure 6F), and remaining $CD44^{hi}GP33^{+}$ cells down-regulated CD69 expression levels (Figure 6G). The frequencies of BM $CD44^{hi}CD8^{+}$ T cells $CXCR3^{+}$, $CD122^{+}$, $NKG2D^{+}$ and $ASGM1^{+}$ cells were also less abundant (Supplementary Fig. 7A). Importantly, the expression level of all these markers was reduced (Supplementary Fig. 7B), suggesting that microbiota stimulation is essential to induce their expression.

These results suggest that the presence of microbiota has an essential role in generation of $CD44^{hi}GP33^{+}CD8^{+}$ T cells, and possibly also $CD44^{hi}CD8^{+}$ T cells with other antigen specificities (Beura et al., 2016; Feng et al., 2010; Kieper et al., 2005). Moreover, microbiota stimulation also influences the properties of $CD44^{hi}$ $CD8^{+}$ T cells.

3.3.3. Microbiota with GP33 molecular mimicry generates $CD44^{hi}GP33^{+}$ $CD8^{+}$ T cells.

A different microbiota composition in different SPF breeding facilities (Thiemann et al., 2017) (or even cages (Constantinides et al., 2019)) can contribute to variable and sometimes contradictory experimental results obtained from genetically identical animals. Therefore, to confirm the role of microbiota in generation of $CD44^{hi}GP33^{+}CD8^{+}$ T cells we

studied B6 mice from another breeding facility (SPF-2). The total number of $CD44^{hi}CD8^{+}$ cells (in SP and BM) were not significant different between mice from the two breeding facilities (Figure 7A). The % and number of $CD44^{hi}OVA^{+}$ cells were also not significant different (not shown). However, the % and total number of $CD44^{hi}GP33^{+}$ were reduced in SP and BM of the SPF-2 (Figure 7B, C). The total number of $CD44^{hi}GP33^{+}$ were reduced 40% in SPF-2 mice. Next, we performed 16S rRNA sequencing from fecal DNA to compare the microbiota composition between the two breeding facilities. Notably, beta diversity revealed a significant difference between the microbiota of SPF-2 and SPF-1, with samples clustering distinctively according to the breeding facility (Figure 7D). Interestingly, bacterial strains predicted to have molecular mimicking with GP33 peptide were significantly decreased in SPF-2 (Figure 7E, F, Supplementary Fig. 8). These results suggest that specific bacteria can promote the generation of some $CD44^{hi}GP33^{+}$ cells in SPF-1 mice. Alpha diversity varied also between the two mouse lines, SPF-2 had lower Shannon diversity index (species richness combined with abundance and evenness) than SPF-1 (Figure 7G, H). Lastly, we found that microbiota stimulation had a continuous effect in $CD44^{hi}GP33^{+}$ cells since their number increase progressively in the BM of SPF-1 mice throughout life (Supplementary Fig. 9).

These results suggest that the presence of microbiota with GP33 molecular mimicry has an essential role in generation of $CD44^{hi}GP33^{+}CD8^{+}$ T cells. The microbiota stimulation is continuous as shown by the selective increase in the number of $CD44^{hi}GP33^{+}$cells throughout life.

3.3.4. Microbiota stimulation is essential for the development of $CD8\alpha\beta^{+}CD44^{hi}GP33^{+}TRBV29^{+}$ intraepithelial lymphocytes.

Intraepithelial lymphocytes (IELs) represent about half of whole lymphocytes of all mouse organism (Rocha et al., 1991). $CD8\alpha\beta^{+}$ $TCR\alpha\beta^{+}$ IELs develop through the continuous

interaction with intestinal antigens such as microbiota (Hegazy et al., 2017; Noble et al., 2019; Regnault et al., 1996; Umesaki et al., 1993). Therefore, we hypothesized that $CD44^{hi}GP33^{+}$ cells would be enriched within the small intestine epithelium of SPF mice (Mani et al., 2019), and express particularly TRBV29/Vβ7. To test this hypothesis, we studied the $CD8\alpha\beta^{+}$ $TCR\alpha\beta^{+}$ IELs of the murine gut of SPF and germ-free (GF) mice. OVA-specific dextramers only detected rare IELs, with very low labelling intensity (Figure 8A middle graphs). By contrast, $CD44^{hi}GP33^{+}CD8\beta^{+}$IELs were clearly identified in SPF-1 mice (Fig. 8A-left lower graphs). In germfree (GF) condition, only very rare events were dispersed in the $CD44^{hi}CD69^{+}GP33^{+}CD8\beta^{+}$ quadrant, i.e., a clear-cut population could not be identified (Figure 8A-right lower graphs). Interestingly, $CD44^{hi}GP33^{+}CD8\beta^{+}$IELs were clearly decreased in SPF-2 mice (Figure 8A-center lower graphs), suggesting that microbiota with GP33 molecular mimicry has an essential role in generation of these cells. The GF condition induced also an overall reduction of $CD44^{hi}CD8^{+}$ cells and $CD44^{hi}GP33^{+}$ cells in gLNs (not shown) and in the lamina propria (LP) (Figure 8B).

The immune response to the LCMV leads to the selection of $GP33^{+}$ cells expressing TRBV29/Vβ7 with a peculiar CASSxxxNxxEQYF CDR3 composition. Lastly, to study if microbiota help in the selection of these TRBV chains we studied the repertoire of the $CD8\alpha\beta^{+}$ $TCR\alpha\beta^{+}$ IELs of SPF mice. Only a minority of $CD8\alpha\beta^{+}$ $TCR\alpha\beta^{+}$ IEL expressed Vβ7 but the vast majority of $CD44^{hi}GP33^{+}$ were $V\beta7^{+}$ (Figure 8C). These data suggest that microbiota exposition can contribute to the selection of $GP33^{+}V\beta7^{+}$ IELs in small intestine of SPF mice. Interestingly, the sequence of the CDR3 region of $GP33^{+}V\beta7^{+}$ IELs of SPF mice showed a CDR3 composition (CASSxxxNxxEQYF), typical of the repertoire of $GP33^{+}$selected during the LCMV response (Figure 8D). Notably, $CD44^{hi}GP33^{+}$ IELs and peripheral $CD44^{hi}GP33^{+}$ shared the dominant features, strongly suggesting that $CD8^{+}$ T cells activated in gut can migrate to the periphery (Beura et al., 2018; Tanoue et al., 2019; Teng et

al., 2016) and be a source of systemic $CD44^{hi}GP33^{+}$ cells. These data suggest that microbiota contribute for the selection of the $GP33^{+}$ $TRBV29^{+}$ during the LCMV infection.

4. Discussion

Microbiota protects against gastrointestinal pathogenic infections, which was named "colonization resistance" effect (Becattini et al., 2017). Microbiota employ an arsenal of mechanisms to influence development and specificity of host innate and adaptive immune system (Belkaid and Harrison, 2017). Therefore, microbiota plays also a crucial role in the prevention and resolution of systemic infections (Becattini et al., 2017; Tanoue et al., 2019). This effect was believed to be indirect. It was described to influence myelopoiesis (Khosravi et al., 2014), to regulate inflammasome activation (Ichinohe et al., 2011) and to promote the production of type I interferon and IFN-γ (Abt et al., 2012; Thiemann et al., 2017). Some studies showed that microbiota generate conventional (Naik et al., 2012) and unconventional (Constantinides et al., 2019; Linehan et al., 2018) skin T cells, increasing their numbers, and these cells support mice skin repair. Recently, certain microbiota components presented by DCs were also shown to generate conventional $CD44^{hi}CD8^{+}$ IFN-γ^{+} cells in the gut and these cells are found also in several peripheral organs (e.g. LNs, SP and lung) (Huggins et al., 2019; Mani et al., 2019; Riquelme et al., 2019; Tanoue et al., 2019). These cells potentiate immune responses to tumours preventing the side effects of anti-PD1 administration (Tanoue et al., 2019). These later results highlight a potential therapeutic role of microbiota, and thus the importance of further studies on the impact of microbiota in immune responses.

We here describe a further major effect of microbiota: helping in the generation of a systemic subpopulation of $CD44^{hi}GP33^{+}CD8^{+}$ T cells that have a major role in the response to LCMV infection. Our results suggest that the heterogeneity and nature of the stimuli responsible for HP and the development of $CD44^{hi}$ $CD8^{+}$ T cells was underestimated in the

previously described cell sets. Since T cells transferred into SCID SPF mice proliferate much more than those transferred to SCID GF hosts (Kieper et al., 2005) microbiota antigens was proposed to have a major role in HP. More recently, it was claimed that microbiota did not have any impact in this phenomenon, HP being strictly dependent on cross-reactivity with self-antigens (Haluszczak et al., 2009; Kawabe et al., 2017; Quinn et al., 2016). Our data suggest that the differences in the TCR cross-reactivity of the cells studied in each experiment explain these opposite conclusions. We found that the OVA peptide mimics self-antigens present in multiple tissues, OVA-specific $CD8^+$ T cells have the classical virtual memory T (T_{VM}) phenotype ($CD44^{hi}CD49d^{low}CD62L^+$) (Haluszczak et al., 2009; White et al., 2016) and are not reduced in the SP of GF mice. The OVA-specific HP $CD44^{hi}CD8^+$ would be generated in conditions of T cell depletion (as found in neonatal and T cell deficient hosts) by the stimulation with cross-reactive self-antigens (Ge et al., 2004; Smith et al., 2018). By contrast, the GP33 peptide has no molecular mimicry with self-antigens but with multiple microbiota components. $CD44^{hi}GP33^+$ cells have a TCR with a CDR3 region inriched in glycines witch lead to greater promiscuity in antigen recognition (Chowell et al., 2015; Stadinski et al., 2016) indicating that these cells have a higher advantage to become activated by cross-reactive microbiota antigens and engaged in HP. Our results suggest that microbiota with GP33 molecular mimicry generates these $CD44^{hi}GP33^+$ $CD8^+$ T cells. $CD44^{hi}GP33^+$ were absent in the IELs of GF mice (where self and food antigens are present), and were hardly detected in other lymphoid organs, further suggest a role of microbiota antigens in their generation. In addition, the continuous microbiota stimulation induce a selective increase in peripheral $CD44^{hi}GP33^+$ cells numbers throughout life (Quinn et al., 2018; Su et al., 2013). Besides $GP33^+$ cells, microbiota stimulation likely affects $CD8^+$ T cells with other antigen specificities, and also influences their properties. The total number of $CD44^{hi}CD8^+$ T cells was reduced by 50% in GF mice and the phenotype of residual $CD44^{hi}CD8^+$ T cells was

modified. The existence of these two sub-types of cross reactive $CD44^{hi}CD8^{+}$ antigen-specific populations is supported by the fact that $CD44^{hi}CD8^{+}$ peripheral T cell pool yet persist in GF conditions and immune responses to OVA are not affected by the absence of microbiota (Haluszczak et al., 2009), while responses to several pathogens (including *Listeria monocytogenes*, Influenza A and LCMV) are much reduced (Abt et al., 2012; Ichinohe et al., 2011; Khosravi et al., 2014; Thackray et al., 2018). In line with a further major effect of microbiota in generation of a systemic subpopulation of $CD44^{hi}GP33^{+}CD8^{+}$ T cells, GF mice that lack the population of $CD44^{hi}GP33^{+}$ T cells, exhibited a significant reduction in the number of effector $GP33^{+}$ T cells in multiple tissues 7 days post-LCMV infection and virus clearance is much delayed (Abt et al., 2012; MC, 2009).

$CD44^{hi}GP33^{+}$ phenotype in SPF mice differs from T_{VM} and T_{RM} (Haluszczak et al., 2009; White et al., 2016). They share multiple characteristics of innate lymphocytes, including a very high expression of several NKRs and CXCR3. The expression of CXCR3 was shown to identify a cell subset able to mediate effector functions in the absence of TCR stimulation (Soudja et al., 2012). Indeed, $CD44^{hi}GP33^{+}$ cells proliferate and express IFN-γ and granzyme B after overnight incubation with the cytokine cocktail, previously used to stimulate innate cells (Haluszczak et al., 2009). NKR receptors also mediate one prominent pathway for the crosstalk between $CD8^{+}$ T cells and surrounding tissues, activating effector functions independently of TCR stimulation (Seyda et al., 2016). Through their ubiquitous high expression of NKG2D activator receptor $CD44^{hi}GP33^{+}$ cells can recognize and be activated by NKG2D ligands. These ligands are poorly expressed in healthy tissues, but are up-regulated on the surface of stressed, malignant or virus-infected cells (Raulet, 2003). Through this receptor, $CD44^{hi}GP33^{+}$ cells may share the capacity of innate lymphoid cells (Seyda et al., 2016; Soudja et al., 2012) to interact with these cells in the absence of TCR recognition. Besides, their expression of activating NKRs confers them antigen-independent

bystander properties against target cells expressing stress markers, as well as a lower their TCR activation threshold (Seyda et al., 2016) allowing them to respond to lower affinity cross-reactive antigens. These $CD44^{hi}GP33^{+}$ cells may act as early sensors to stress signals. Lastly, $CD44^{hi}GP33^{+}$ cells expressed receptors allowing their direct stimulation microbiota. Their glycolipid receptor ASGM1 confers the capacity to respond to flagellin (McNamara et al., 2001), a major component of gram-negative bacteria. A fraction of $CD44^{hi}GP33^{+}$ and of total $CD44^{hi}CD8^{+}$ also expresses TLR4, suggesting that may be directly stimulated by bacterial LPS. It was shown that TLR4 can be expressed on the surface of activated mouse $CD8^{+}$ T cells (Huggins et al., 2019; Loser et al., 2010) and TLR4 activation enhances $CD8^{+}$ T cell proliferation, cytokine production and cytotoxicity (Wang et al., 2019). For example, microbiota exposition increase numbers of $CD44^{hi}CD8^{+}$ T cells and $CD44^{hi}CD8^{+}$ T expressing TLR4 (Huggins et al., 2019), but the $CD8^{+}$ sub-population expressing TLR4 was not characterized further.

SPF mice harbour $CD44^{hi}GP33^{+}$ cells in SP, LN, LP, IELs and BM. However, $CD44^{hi}GP33^{+}$ cells were particularly abundant in the BM of unmanipulated SPF mice. It must be noted that $GP33^{+}CD44^{hi}$ populations located in the BM cannot be considered T_{RM} since parabiosis experiments demonstrated that all $CD8^{+}$ T cells (including $CD44^{hi}CD69^{+}CD8^{+}$ T cells) present in the BM recirculate in-between different organs: they reach full chimerism in the two mice connected in each parabiotic pair (Klonowski et al., 2004; Stark et al., 2018; Thomas et al., 2011). We observed that $CD44^{hi}GP33^{+}$ cells are selected during primary LCMV infection in SPF mice, as shown by their precocious accumulation, increased division and survival in the BM, where $CD44^{hi}GP33^{+}$ cells predominate. These results show that the BM must also be considered as a secondary lymphoid organ with a major role even in the primary immune responses (Duffy et al., 2012; Feuerer et al., 2003). $CD44^{hi}GP33^{+}$ cells are poised for greater bursts of proliferation when they encounter the antigen (Smith et al., 2018),

and they dominate the immune response to LCMV infection (Fulton et al., 2015). We here describe that the TCR repertoire of $GP33^+$ cells during LCMV response shifts from that of naïve $CD44^-GP33^+$ (where $V\beta8^+$ cells predominate) to the repertoire of $CD44^{hi}GP33^+$ cells particularly those expressing TRBV29/$V\beta7^+$. We envisaged that microbiota stimulation could be responsible for the preferential selection of TRBV29/$V\beta7^+$ CASSxxNxxEQYF $GP33^+$ during the LCMV response. To evaluate this possibility we studied the repertoire of $TCR\alpha\beta^+$ $GP33^+$ IELs from SPF mice, which are in contact with microbiota, but are not stimulated by LCMV. We found selection mechanisms overlapping those found in the peripheral pools during the LCMV response. While the majority of IELs did not express Vβ7, the vast majority of $GP33^+$ IELs expressed Vβ7. Importantly, the CDR3 domains of $GP33^+V\beta7^+$ IELs of SPF mice had the CASSxxNxxEQYF motif found in the $GP33^+V\beta7^+$ selected in the peripheral T cell pools after LCMV infection. Taking into consideration the potential heterogeneity of TCRβ repertoires (Goncalves et al., 2017), the expression of equivalent TRBV chains in $GP33^+$ IELs of SPF mice and in $GP33^+$ peripheral T cells selected during LCMV infection can only be explained by a common selection mechanism. Interestingly, microbiota-reactive T cells were also prevalent in the human gut mucosa (Hegazy et al., 2017; Noble et al., 2019), and some circulating memory T cells recognize the same peptides derived from gut bacteria and can cross-react to other pathogens (Borbulevych et al., 2009; Hegazy et al., 2017; Noble et al., 2019; Su et al., 2013). These results suggest that microbiota can induce the expansion of antigen-specific memory phenotypic T cells in gut and periphery of both mice and human (Su et al., 2013).

Lastly, the influence of microbiota in the generation $CD44^{hi}GP33^+$ cells must also be addressed. Microbiota antigens are continuously recognized by the adaptive immune system during homeostasis and some studies showed that mice antigen-specific T cells can have cross-reactivity to microbial mimotopes and be activated by these antigens (Beura et al.,

2016; Gil-Cruz et al., 2019; Harkiolaki et al., 2009; Tanoue et al., 2019; Yang et al., 2014). However, further studies will be required to investigate if microbiota mimotopes directly prime naïve $CD44^{-}GP33^{+}$ cells induce their activation and promote the generation of $CD44^{hi}GP33^{+}$ T cells in SPF mice. For example, microbiota can also regulate certain antigen-presenting cells and affect cross-presentation (Khosravi et al., 2014). In addition to mimotopes, microbiota-derived ligands (e.g. LPS) can also enter the systemic blood circulation induce innate stimulation (Feng et al., 2010) and promote bystander activation and proliferation/survival of $CD44^{hi}$ $CD8^{+}$ T cells (Tough et al., 1997). Besides structural components of bacteria, many of metabolites derived from microbiota metabolism (e.g. short-chain fatty acids, vitamins, bile acids, sterols, and xenobiotics) have been implicated in the development and function of diverse immune cells including antigen-presenting cells and $CD8^{+}$ T cells (Tanoue et al., 2019). Both microbiota-induced antigen-specific $CD8^{+}$ T cells activation and microbiota innate stimulation-driven $CD44^{hi}$ $CD8^{+}$ T cells proliferation and survival may be required for the generation/maintenance of innate $CD44^{hi}GP33^{+}$ cells. In addition, cytokines stimulation were also involved in this process (Haluszczak et al., 2009; White et al., 2016).

To summarize, these results suggest a novel and direct function of microbiota in antigen-specific cells, which has a major impact in response to virus infection. This data suggest that microbiota components are responsible for the generation of a sub-population of $CD44^{hi}CD8^{+}$ T cells in SPF mice, which can function as “innate guardians” to multiple types of aggressions. Besides, microbiota also plays a major role in the response of $CD8^{+}$ T cells and in the selection of their TCRβ repertoire during the response to LCMV infection. Microbiota can primes the peripheral T cell pools of naïve mice providing a pool of cross-reactive pre-activated memory cells that improve the efficiency of primary immune responses to virus infection.

Conflict of interest: The authors declare no competing financial interests.

Acknowledgments.

We thank members of the Di Santo laboratory for discussions. We would also like to thank Antonio Bandeira for scientific discussion, suggestions and for critical reading of the manuscript. We thank the members of Biomics NGS platform of the Institut Pasteur, Sean Kennedy and Laurence Motreff for microbial sequencing, and Amine Ghozlane and Emna Achouri for the assistance with the data analysis. The European Union Seventh Framework Programme (FP7/2007-2013) under grant agreement 317040 (ITN QuanTI) funded this study, and the researchers P. Gonçalves and S. el Daker. P. Gonçalves is currently supported by a Grant from the "Labex Milieu Intérieur" ANR 10-LBX-69 MI (http://www.milieuinterieur.fr/en). This study was also partially supported by grants from the Institut Pasteur, INSERM, ANR (15-CE15-000- ILC3_MEMORY) and ERC (695467-ILC_REACTIVITY).

P.G. conducted most of the experiments, analyzed the data and prepared the manuscript. S.D., F.V., N.S., A.L. D.G. and O.A. performed experiments. H.D. prepared and titrated the LCMV virus. D.G, J.S., A.F and B.R. designed experiments and prepared the manuscript.

Appendix A. Supplementary data: Supplementary data associated with this article can be found, in the online version, at…

5. References

Abt, M.C., Osborne, L.C., Monticelli, L.A., Doering, T.A., Alenghat, T., Sonnenberg, G.F., Paley, M.A., Antenus, M., Williams, K.L., Erikson, J., Wherry, E.J., Artis, D., 2012. Commensal Bacteria Calibrate the Activation Threshold of Innate Antiviral Immunity. Immunity 37, 158-170.

Adams, J.J., Narayanan, S., Birnbaum, M.E., Sidhu, S.S., Blevins, S.J., Gee, M.H., Sibener, L.V., Baker, B.M., Kranz, D.M., Garcia, K.C., 2016. Structural interplay between germline interactions and adaptive recognition determines the bandwidth of TCR-peptide-MHC cross-reactivity. Nat Immunol 17, 87-+.

Becattini, S., Littmann, E.R., Carter, R.A., Kim, S.G., Morjaria, S.M., Ling, L., Gyaltshen, Y., Fontana, E., Taur, Y., Leiner, I.M., Pamer, E.G., 2017. Commensal microbes provide first line defense against Listeria monocytogenes infection. J Exp Med 214, 1973-1989.

Belkaid, Y., Harrison, O.J., 2017. Homeostatic Immunity and the Microbiota. Immunity 46, 562-576.

Beura, L.K., Hamilton, S.E., Bi, K., Schenkel, J.M., Odumade, O.A., Casey, K.A., Thompson, E.A., Fraser, K.A., Rosato, P.C., Filali-Mouhim, A., Sekaly, R.P., Jenkins, M.K., Vezys, V., Haining, W.N., Jameson, S.C., Masopust, D., 2016. Normalizing the environment recapitulates adult human immune traits in laboratory mice. Nature 532, 512-+.

Beura, L.K., Wijeyesinghe, S., Thompson, E.A., Macchietto, M.G., Rosato, P.C., Pierson, M.J., Schenkel, J.M., Mitchell, J.S., Vezys, V., Fife, B.T., Shen, S., Masopust, D., 2018. T Cells in Nonlymphoid Tissues Give Rise to Lymph-Node-Resident Memory T Cells. Immunity 48, 327-338 e325.

Birnbaum, M.E., Mendoza, J.L., Sethi, D.K., Dong, S., Glanville, J., Dobbins, J., Ozkan, E., Davis, M.M., Wucherpfennig, K.W., Garcia, K.C., 2014. Deconstructing the Peptide-MHC Specificity of T Cell Recognition. Cell 157, 1073-1087.

Borbulevych, O.Y., Piepenbrink, K.H., Gloor, B.E., Scott, D.R., Sommese, R.F., Cole, D.K., Sewell, A.K., Baker, B.M., 2009. T cell receptor cross-reactivity directed by antigen-dependent tuning of peptide-MHC molecular flexibility. Immunity 31, 885-896.

Chowell, D., Krishna, S., Becker, P.D., Cocita, C., Shu, J., Tan, X.F., Greenberg, P.D., Klavinskis, L.S., Blattman, J.N., Anderson, K.S., 2015. TCR contact residue hydrophobicity is a hallmark of immunogenic CD8(+) T cell epitopes. P Natl Acad Sci USA 112, E1754-E1762.

Cole, D.K., Yuan, F., Rizkallah, P.J., Miles, J.J., Gostick, E., Price, D.A., Gao, G.F., Jakobsen, B.K., Sewell, A.K., 2009. Germ Line-governed Recognition of a Cancer Epitope by an Immunodominant Human T-cell Receptor. Journal of Biological Chemistry 284, 27281-27289.

Constantinides, M.G., Link, V.M., Tamoutounour, S., Wong, A.C., Perez-Chaparro, P.J., Han, S.J., Chen, Y.E., Li, K., Farhat, S., Weckel, A., Krishnamurthy, S.R., Vujkovic-Cvijin, I., Linehan, J.L., Bouladoux, N., Merrill, E.D., Roy, S., Cua, D.J., Adams, E.J., Bhandoola, A., Scharschmidt, T.C., Aube, J., Fischbach, M.A., Belkaid, Y., 2019. MAIT cells are imprinted by the microbiota in early life and promote tissue repair. Science 366.

Das, D.K., Feng, Y., Mallis, R.J., Li, X., Keskin, D.B., Hussey, R.E., Brady, S.K., Wang, J.H., Wagner, G., Reinherz, E.L., Lang, M.J., 2015. Force-dependent transition in the T-cell receptor beta-subunit allosterically regulates peptide discrimination and pMHC bond lifetime. Proc Natl Acad Sci U S A 112, 1517-1522.

Debes, G.F., Arnold, C.N., Young, A.J., Krautwald, S., Lipp, M., Hay, J.B., Butcher, E.C., 2005. Chemokine receptor CCR7 required for T lymphocyte exit from peripheral tissues. Nat Immunol 6, 889-894.

Drobek, A., Moudra, A., Mueller, D., Huranova, M., Horkova, V., Pribikova, M., Ivanek, R., Oberle, S., Zehn, D., McCoy, K.D., Draber, P., Stepanek, O., 2018. Strong homeostatic TCR signals induce formation of self-tolerant virtual memory CD8 T cells. The EMBO journal 37.
Duffy, D., Perrin, H., Abadie, V., Benhabiles, N., Boissonnas, A., Liard, C., Descours, B., Reboulleau, D., Bonduelle, O., Verrier, B., Van Rooijen, N., Combadiere, C., Combadiere, B., 2012. Neutrophils Transport Antigen from the Dermis to the Bone Marrow, Initiating a Source of Memory CD8(+) T Cells (Vol 37, Pg 917, 2012). Immunity 37, 1145-1145.
Esterhazy, D., Canesso, M.C.C., Mesin, L., Muller, P.A., de Castro, T.B.R., Lockhart, A., ElJalby, M., Faria, A.M.C., Mucida, D., 2019. Compartmentalized gut lymph node drainage dictates adaptive immune responses. Nature 569, 126-130.
Feng, T., Wang, L., Schoeb, T.R., Elson, C.O., Cong, Y., 2010. Microbiota innate stimulation is a prerequisite for T cell spontaneous proliferation and induction of experimental colitis. J Exp Med 207, 1321-1332.
Feuerer, M., Beckhove, P., Garbi, N., Mahnke, Y., Limmer, A., Hommel, M., Hammerling, G.J., Kyewski, B., Hamann, A., Umansky, V., Schirrmacher, V., 2003. Bone marrow as a priming site for T-cell responses to blood-borne antigen. Nat Med 9, 1151-1157.
Freitas, A.A., Rocha, B., 2000. Population biology of lymphocytes: the flight for survival. Annual review of immunology 18, 83-111.
Fulton, R.B., Hamilton, S.E., Xing, Y., Best, J.A., Goldrath, A.W., Hogquist, K.A., Jameson, S.C., 2015. The TCR's sensitivity to self peptide-MHC dictates the ability of naive CD8(+) T cells to respond to foreign antigens. Nat Immunol 16, 107-117.
Ge, Q., Bai, A.L., Jones, B., Eisen, H.N., Chen, J.Z., 2004. Competition for self-peptide-MHC complexes and cytokines between naive and memory CD8(+) T cells expressing the same or different T cell receptors. P Natl Acad Sci USA 101, 3041-3046.
Gil-Cruz, C., Perez-Shibayama, C., De Martin, A., Ronchi, F., van der Borght, K., Niederer, R., Onder, L., Lutge, M., Novkovic, M., Nindl, V., Ramos, G., Arnoldini, M., Slack, E.M.C., Boivin-Jahns, V., Jahns, R., Wyss, M., Mooser, C., Lambrecht, B.N., Maeder, M.T., Rickli, H., Flatz, L., Eriksson, U., Geuking, M.B., McCoy, K.D., Ludewig, B., 2019. Microbiota-derived peptide mimics drive lethal inflammatory cardiomyopathy. Science 366, 881-886.
Goncalves, P., Ferrarini, M., Molina-Paris, C., Lythe, G., Vasseur, F., Lim, A., Rocha, B., Azogui, O., 2017. A new mechanism shapes the naive CD8+ T cell repertoire: The selection for full diversity. Molecular immunology 85, 66-80.
Guy-Grand, D., Vassalli, P., Eberl, G., Pereira, P., Burlen-Defranoux, O., Lemaitre, F., Di Santo, J.P., Freitas, A.A., Cumano, A., Bandeira, A., 2013. Origin, trafficking, and intraepithelial fate of gut-tropic T cells (vol 210, pg 1839, 2013). J Exp Med 210, 2493-2493.
Haluszczak, C., Akue, A.D., Hamilton, S.E., Johnson, L.D.S., Pujanauski, L., Teodorovic, L., Jameson, S.C., Kedl, R.M., 2009. The antigen-specific CD8(+) T cell repertoire in unimmunized mice includes memory phenotype cells bearing markers of homeostatic expansion. J Exp Med 206, 435-448.
Hao, Y., Legrand, N., Freitas, A.A., 2006. The clone size of peripheral CD8 T cells is regulated by TCR promiscuity. J Exp Med 203, 1643-1649.
Harkiolaki, M., Holmes, S.L., Svendsen, P., Gregersen, J.W., Jensen, L.T., McMahon, R., Friese, M.A., van Boxel, G., Etzensperger, R., Tzartos, J.S., Kranc, K., Sainsbury, S., Harlos, K., Mellins, E.D., Palace, J., Esiri, M.M., van der Merwe, P.A., Jones, E.Y., Fugger, L., 2009. T cell-mediated autoimmune disease due to low-affinity crossreactivity to common microbial peptides. Immunity 30, 348-357.
Hegazy, A.N., West, N.R., Stubbington, M.J.T., Wendt, E., Suijker, K.I.M., Datsi, A., This, S., Danne, C., Campion, S., Duncan, S.H., Owens, B.M.J., Uhlig, H.H., McMichael, A., Bergthaler, A., Teichmann, S.A., Keshav, S., Powrie, F., 2017. Circulating and Tissue-Resident CD4(+) T Cells With Reactivity to Intestinal Microbiota Are Abundant in Healthy

Individuals and Function Is Altered During Inflammation. Gastroenterology 153, 1320-1337 e1316.
Huggins, M.A., Sjaastad, F.V., Pierson, M., Kucaba, T.A., Swanson, W., Staley, C., Weingarden, A.R., Jensen, I.J., Danahy, D.B., Badovinac, V.P., Jameson, S.C., Vezys, V., Masopust, D., Khoruts, A., Griffith, T.S., Hamilton, S.E., 2019. Microbial Exposure Enhances Immunity to Pathogens Recognized by TLR2 but Increases Susceptibility to Cytokine Storm through TLR4 Sensitization. Cell Rep 28, 1729-+.
Ichinohe, T., Pang, I.K., Kumamoto, Y., Peaper, D.R., Ho, J.H., Murray, T.S., Iwasaki, A., 2011. Microbiota regulates immune defense against respiratory tract influenza A virus infection. P Natl Acad Sci USA 108, 5354-5359.
Jaravine, V., Raffegerst, S., Schendel, D.J., Frishman, D., 2017. Assessment of cancer and virus antigens for cross-reactivity in human tissues. Bioinformatics 33, 104-111.
Kawabe, T., Jankovic, D., Kawabe, S., Huang, Y., Lee, P.H., Yamane, H., Zhu, J., Sher, A., Germain, R.N., Paul, W.E., 2017. Memory-phenotype CD4+ T cells spontaneously generated under steady-state conditions exert innate TH1-like effector function. Science immunology 2.
Khosravi, A., Yanez, A., Price, J.G., Chow, A., Merad, M., Goodridge, H.S., Mazmanian, S.K., 2014. Gut Microbiota Promote Hematopoiesis to Control Bacterial Infection. Cell host & microbe 15, 374-381.
Kieper, W.C., Troy, A., Burghardt, J.T., Ramsey, C., Lee, J.Y., Jiang, H.Q., Dummer, W., Shen, H., Cebra, J.J., Surh, C.D., 2005. Cutting edge: Recent immune status determines the source of antigens that drive homeostatic T cell expansion. Journal of Immunology 174, 3158-3163.
Klonowski, K.D., Williams, K.J., Marzo, A.L., Blair, D.A., Lingenheld, E.G., Lefrancois, L., 2004. Dynamics of blood-borne CD8 memory T cell migration in vivo. Immunity 20, 551-562.
Lee, J.Y., Hamilton, S.E., Akue, A.D., Hogquist, K.A., Jameson, S.C., 2013. Virtual memory CD8 T cells display unique functional properties. P Natl Acad Sci USA 110, 13498-13503.
Li, N., van Unen, V., Abdelaal, T., Guo, N., Kasatskaya, S.A., Ladell, K., McLaren, J.E., Egorov, E.S., Izraelson, M., Chuva de Sousa Lopes, S.M., Hollt, T., Britanova, O.V., Eggermont, J., de Miranda, N., Chudakov, D.M., Price, D.A., Lelieveldt, B.P.F., Koning, F., 2019. Memory CD4(+) T cells are generated in the human fetal intestine. Nat Immunol.
Linehan, J.L., Harrison, O.J., Han, S.J., Byrd, A.L., Vujkovic-Cvijin, I., Villarino, A.V., Sen, S.K., Shaik, J., Smelkinson, M., Tamoutounour, S., Collins, N., Bouladoux, N., Dzutsev, A., Rosshart, S.P., Arbuckle, J.H., Wang, C.R., Kristie, T.M., Rehermann, B., Trinchieri, G., Brenchley, J.M., O'Shea, J.J., Belkaid, Y., 2018. Non-classical Immunity Controls Microbiota Impact on Skin Immunity and Tissue Repair. Cell 172, 784-+.
Loser, K., Vogl, T., Voskort, M., Lueken, A., Kupas, V., Nacken, W., Klenner, L., Kuhn, A., Foell, D., Sorokin, L., Luger, T.A., Roth, J., Beissert, S., 2010. The Toll-like receptor 4 ligands Mrp8 and Mrp14 are crucial in the development of autoreactive CD8(+) T cells. Nat Med 16, 713-U119.
Mani, V., Bromley, S.K., Aijo, T., Mora-Buch, R., Carrizosa, E., Warner, R.D., Hamze, M., Sen, D.R., Chasse, A.Y., Lorant, A., Griffith, J.W., Rahimi, R.A., McEntee, C.P., Jeffrey, K.L., Marangoni, F., Travis, M.A., Lacy-Hulbert, A., Luster, A.D., Mempel, T.R., 2019. Migratory DCs activate TGF-beta to precondition naive CD8(+) T cells for tissue-resident memory fate. Science 366.
MC, A., 2009. The influence of commensal bacteria on anti-viral immunity. J Immunol.
McNamara, N., Khong, A., McKemy, D., Caterina, M., Boyer, J., Julius, D., Basbaum, C., 2001. ATP transducer signals from ASGM1, a glycolipid that functions as a bacterial receptor. P Natl Acad Sci USA 98, 9086-9091.

Murali-Krishna, K., Altman, J.D., Suresh, M., Sourdive, D.J., Zajac, A.J., Miller, J.D., Slansky, J., Ahmed, R., 1998. Counting antigen-specific CD8 T cells: a reevaluation of bystander activation during viral infection. Immunity 8, 177-187.
Naik, S., Bouladoux, N., Wilhelm, C., Molloy, M.J., Salcedo, R., Kastenmuller, W., Deming, C., Quinones, M., Koo, L., Conlan, S., Spencer, S., Hall, J.A., Dzutsev, A., Kong, H., Campbell, D.J., Trinchieri, G., Segre, J.A., Belkaid, Y., 2012. Compartmentalized control of skin immunity by resident commensals. Science 337, 1115-1119.
Noble, A., Durant, L., Hoyles, L., McCartney, A.L., Man, R., Segal, J., Costello, S.P., Hendy, P., Reddi, D., Bouri, S., Lim, D.N.F., Pring, T., O'Connor, M.J., Datt, P., Wilson, A., Arebi, N., Akbar, A., Hart, A.L., Carding, S.R., Knight, S.C., 2019. Deficient Resident Memory T-Cell and Cd8 T-Cell Response to Commensals in Inflammatory Bowel Disease. J Crohns Colitis.
Pascutti, M.F., Geerman, S., Collins, N., Brasser, G., Nota, B., Stark, R., Behr, F., Oja, A., Slot, E., Panagioti, E., Prier, J.E., Hickson, S., Wolkers, M.C., Heemskerk, M.H.M., Hombrink, P., Arens, R., Mackay, L.K., van Gisbergen, K., Nolte, M.A., 2019. Peripheral and systemic antigens elicit an expandable pool of resident memory CD8(+) T cells in the bone marrow. European journal of immunology 49, 853-872.
Quereda, J.J., Dussurget, O., Nahori, M.A., Ghozlane, A., Volant, S., Dillies, M.A., Regnault, B., Kennedy, S., Mondot, S., Villoing, B., Cossart, P., Pizarro-Cerda, J., 2016. Bacteriocin from epidemic Listeria strains alters the host intestinal microbiota to favor infection. P Natl Acad Sci USA 113, 5706-5711.
Quinn, K.M., Fox, A., Harland, K.L., Russ, B.E., Li, J., Nguyen, T.H.O., Loh, L., Olshanksy, M., Naeem, H., Tsyganov, K., Wiede, F., Webster, R., Blyth, C., Sng, X.Y.X., Tiganis, T., Powell, D., Doherty, P.C., Turner, S.J., Kedzierska, K., La Gruta, N.L., 2018. Age-Related Decline in Primary CD8(+) T Cell Responses Is Associated with the Development of Senescence in Virtual Memory CD8(+) T Cells. Cell Rep 23, 3512-3524.
Quinn, K.M., Zaloumis, S.G., Cukalac, T., Kan, W.T., Sng, X.Y., Mirams, M., Watson, K.A., McCaw, J.M., Doherty, P.C., Thomas, P.G., Handel, A., La Gruta, N.L., 2016. Heightened self-reactivity associated with selective survival, but not expansion, of naive virus-specific CD8+ T cells in aged mice. Proc Natl Acad Sci U S A.
Raue, H.P., Beadling, C., Haun, J., Slifka, M.K., 2013. Cytokine-mediated programmed proliferation of virus-specific CD8(+) memory T cells. Immunity 38, 131-139.
Raulet, D.H., 2003. Roles of the NKG2D immunoreceptor and its ligands. Nat Rev Immunol 3, 781-790.
Regnault, A., Levraud, J.P., Lim, A., Six, A., Moreau, C., Cumano, A., Kourilsky, P., 1996. The expansion and selection of T cell receptor alpha beta intestinal intraepithelial T cell clones. European journal of immunology 26, 914-921.
Riquelme, E., Zhang, Y., Zhang, L.L., Montiel, M., Zoltan, M., Dong, W.L., Quesada, P., Sahin, I., Chandra, V., San Lucas, A., Scheet, P., Xu, H.W., Hanash, S.M., Feng, L., Burks, J.K., Do, K.A., Peterson, C.B., Nejman, D., Tzeng, C.W.D., Kim, M.P., Sears, C.L., Ajami, N., Petrosino, J., Wood, L.D., Maitra, A., Straussman, R., Katz, M., White, J.R., Jenq, R., Wargo, J., McAllister, F., 2019. Tumor Microbiome Diversity and Composition Influence Pancreatic Cancer Outcomes. Cell 178, 795-+.
Rocha, B., Vassalli, P., Guy-Grand, D., 1991. The V beta repertoire of mouse gut homodimeric alpha CD8+ intraepithelial T cell receptor alpha/beta + lymphocytes reveals a major extrathymic pathway of T cell differentiation. J Exp Med 173, 483-486.
Seyda, M., Elkhal, A., Quante, M., Falk, C.S., Tullius, S.G., 2016. T Cells Going Innate. Trends Immunol 37, 546-556.
Slifka, M.K., Matloubian, M., Ahmed, R., 1995. Bone-Marrow Is a Major Site of Long-Term Antibody-Production after Acute Viral-Infection. Journal of virology 69, 1895-1902.

Smith, N.L., Patel, R.K., Reynaldi, A., Grenier, J.K., Wang, J., Watson, N.B., Nzingha, K., Yee Mon, K.J., Peng, S.A., Grimson, A., Davenport, M.P., Rudd, B.D., 2018. Developmental Origin Governs CD8(+) T Cell Fate Decisions during Infection. Cell 174, 117-130 e114.
Soudja, S.M., Ruiz, A.L., Marie, J.C., Lauvau, G., 2012. Inflammatory Monocytes Activate Memory CD8(+) T and Innate NK Lymphocytes Independent of Cognate Antigen during Microbial Pathogen Invasion. Immunity 37, 549-562.
Stadinski, B.D., Shekhar, K., Gomez-Tourino, I., Jung, J., Sasaki, K., Sewell, A.K., Peakman, M., Chakraborty, A.K., Huseby, E.S., 2016. Hydrophobic CDR3 residues promote the development of self-reactive T cells. Nat Immunol.
Stark, R., Wesselink, T.H., Behr, F.M., Kragten, N.A.M., Arens, R., Koch-Nolte, F., van Gisbergen, K., van Lier, R.A.W., 2018. T RM maintenance is regulated by tissue damage via P2RX7. Science immunology 3.
Su, L.F., Kidd, B.A., Han, A., Kotzin, J.J., Davis, M.M., 2013. Virus-specific CD4(+) memory-phenotype T cells are abundant in unexposed adults. Immunity 38, 373-383.
Sung, H.C., Lemos, S., Ribeiro-Santos, P., Kozyrytska, K., Vasseur, F., Legrand, A., Charbit, A., Rocha, B., Evaristo, C., 2013. Cognate antigen stimulation generates potent CD8(+) inflammatory effector T cells. Frontiers in immunology 4, 452.
Surh, C.D., Sprent, J., 2000. Homeostatic T cell proliferation: How far can T cells be activated to self-ligands? J Exp Med 192, F9-F14.
Tanoue, T., Morita, S., Plichta, D.R., Skelly, A.N., Suda, W., Sugiura, Y., Narushima, S., Vlamakis, H., Motoo, I., Sugita, K., Shiota, A., Takeshita, K., Yasuma-Mitobe, K., Riethmacher, D., Kaisho, T., Norman, J.M., Mucida, D., Suematsu, M., Yaguchi, T., Bucci, V., Inoue, T., Kawakami, Y., Olle, B., Roberts, B., Hattori, M., Xavier, R.J., Atarashi, K., Honda, K., 2019. A defined commensal consortium elicits CD8 T cells and anti-cancer immunity. Nature.
Teng, F., Klinger, C.N., Felix, K.M., Bradley, C.P., Wu, E., Tran, N.L., Umesaki, Y., Wu, H.J.J., 2016. Gut Microbiota Drive Autoimmune Arthritis by Promoting Differentiation and Migration of Peyer's Patch T Follicular Helper Cells. Immunity 44, 875-888.
Thackray, L.B., Handley, S.A., Gorman, M.J., Poddar, S., Bagadia, P., Briseno, C.G., Theisen, D.J., Tan, Q., Hykes, B.L., Jr., Lin, H., Lucas, T.M., Desai, C., Gordon, J.I., Murphy, K.M., Virgin, H.W., Diamond, M.S., 2018. Oral Antibiotic Treatment of Mice Exacerbates the Disease Severity of Multiple Flavivirus Infections. Cell Rep 22, 3440-3453 e3446.
Thiemann, S., Smit, N., Roy, U., Lesker, T.R., Galvez, E.J.C., Helmecke, J., Basic, M., Bleich, A., Goodman, A.L., Kalinke, U., Flavell, R.A., Erhardt, M., Strowig, T., 2017. Enhancement of IFNgamma Production by Distinct Commensals Ameliorates Salmonella-Induced Disease. Cell Host Microbe 21, 682-694 e685.
Thomas, S.Y., Scanlon, S.T., Griewank, K.G., Constantinides, M.G., Savage, A.K., Barr, K.A., Meng, F.Y., Luster, A.D., Bendelac, A., 2011. PLZF induces an intravascular surveillance program mediated by long-lived LFA-1-ICAM-1 interactions. J Exp Med 208, 1179-1188.
Tough, D.F., Sun, S.Q., Sprent, J., 1997. T cell stimulation in vivo by lipopolysaccharide (LPS). J Exp Med 185, 2089-2094.
Turner, S.J., Doherty, P.C., McCluskey, J., Rossjohn, J., 2006. Structural determinants of T-cell receptor bias in immunity. Nat Rev Immunol 6, 883-894.
Umesaki, Y., Setoyama, H., Matsumoto, S., Okada, Y., 1993. Expansion of Alpha-Beta T-Cell Receptor-Bearing Intestinal Intraepithelial Lymphocytes after Microbial Colonization in Germ-Free Mice and Its Independence from Thymus. Immunology 79, 32-37.
Veiga-Fernandes, H., Walter, U., Bourgeois, C., McLean, A., Rocha, B., 2000. Response of naive and memory CD8(+) T cells to antigen stimulation in vivo. Nat Immunol 1, 47-53.

Wang, Y., Chung, Y.R., Eitzinger, S., Palacio, N., Gregory, S., Bhattacharyya, M., Penaloza-MacMaster, P., 2019. TLR4 signaling improves PD-1 blockade therapy during chronic viral infection. Plos Pathog 15, e1007583.
White, J.T., Cross, E.W., Burchill, M.A., Danhorn, T., McCarter, M.D., Rosen, H.R., O'Connor, B., Kedl, R.M., 2016. Virtual memory T cells develop and mediate bystander protective immunity in an IL-15-dependent manner. Nature communications 7.
White, J.T., Cross, E.W., Kedl, R.M., 2017. Antigen-inexperienced memory CD8(+) T cells: where they come from and why we need them. Nature Reviews Immunology 17, 391-400.
Yang, Y., Torchinsky, M.B., Gobert, M., Xiong, H., Xu, M., Linehan, J.L., Alonzo, F., Ng, C., Chen, A., Lin, X., Sczesnak, A., Liao, J.J., Torres, V.J., Jenkins, M.K., Lafaille, J.J., Littman, D.R., 2014. Focused specificity of intestinal TH17 cells towards commensal bacterial antigens. Nature 510, 152-156.

Table legend

Table 1 - The diversity of GP33-specific $CD8^+$ T cells in primary effector phase, memory and secondary effector phase after LCMV infection.

$CD8^+GP33^+$ cells from different LCMV infected mice were sorted from the SP, LN and BM to evaluate *Tcrb* expression in each individual cell from at different time points after LCMV infection. Results show a representative mouse at each time point. Remaining mice and full TCRB sequences of all individual cells in all mice are shown in Table S2. From left to right: the CDR3 region; CDR3 size; *Trbv* gene; *Trbj* genes; the number of cells expressing the same TCRB, localized in a single organ (SP or LN or BM) (**localized**) or present in different organs (**spread**).

Figure legends

Figure 1. $CD44^{hi}GP33^{+}CD8^{+}$ cells from SPF mice express a different phenotype from virtual memory cells ($CD69^{-}CD62L^{+}CD49d^{low}$) or tissue resident memory cells (TRMs) ($CD69^{+}CD62L^{-}CCR7^{-}$). (**A**-**C**, **E**) Results compare the expression of different cell surface markers in gated $CD44^{-}GP33^{+}$ **(black histograms)** and $CD44^{hi}GP33^{+}$ T cells **(red histograms)** from the spleen (SP) of the same mouse. We focus or phenotypic analysis in the SP since the numbers of $CD44^{-}GP33^{+}$ recovered from the BM sometimes were insufficient to allow an accurate comparison between $CD44^{-}$ and $CD44^{hi}GP33^{+}$ cells in the same organ. The numbers in each histogram show the average percentage of positive cells from 4-8 12 weeks old SPF B6 mice, studied in three independent experiments: **upper numbers**: $CD44^{-}GP33^{+}$; **lower numbers**: $CD44^{hi}GP33^{+}$. B and C, $p \leq 0.05$ using the Mann Whitney U-test; **D**: CD69 and CD103 co-expression by total bone marrow (BM) $CD44^{hi}CD8^{+}$T cells.

Figure 2. $CD44^{hi}GP33^{+}CD8^{+}$ T cells from SPF mice express markers of innate lymphocytes. A: MFI of different markers expressed by $CD44^{-}GP33^{+}$ **(black bars)** and $CD44^{hi}GP33^{+}$ T cells **(grey bars).** Results show the mean+/-SEM from 4-8 mice studied in three independent experiments. The differences determined using the Mann Whitney U-test are: $*p \leq 0.05$, $*** p \leq 0.001$. **B:** Histograms compare the expression of different cell surface markers in gated $CD44^{-}GP33^{+}$ **(black lines)** and $CD44^{hi}GP33^{+}$ SP T cells **(read lines)** of the same mouse. The numbers in each histogram show the average percentage of positive cells obtained from 4-8 mice, studied in three independent experiments: $CD44^{-}GP33^{+}$ (**upper numbers**) and $CD44^{hi}GP33^{+}$ **(lower numbers)**. All markers $p \leq 0.05$ using the Mann Whitney U-test; **C:** Expression of TLR4 on total $CD44^{hi}CD8^{+}$T cells.

Figure 3. CD44^{hi} GP33^{+} CD8^{+} T cells present in SPF mice share properties of innate lymphocytes. A: Results compare CXCR3, CD121a, CD218a, and CD122 expression by CD44^{-} (black line) and CD44^{hi}GP33^{+} (red line) from the SP of same mouse. The numbers in each histogram show the average percentage of positive cells obtained from 4-8 mice, studied in three independent experiments: CD44^{-}GP33^{+} (**upper numbers**) and CD44^{hi}GP33^{+} **(lower numbers)**. All markers $p \leq 0.05$ using the Mann Whitney U-test. **B: Mean+/- SEM** of the MFI of these markers expression by CD44^{-} (black bars) and CD44^{hi} (grey bars) GP33^{+} cells in 5 mice studied in 3 experiments **C-E:** A pool of CD44^{-} and CD44^{hi} CD8^{+} T cells from SP and BM of SPF mice were sorted and cultured overnight with cytokines. BFA was added for the last 3 h of culture. **C:** Number of GP33^{+} cells in CD44^{-} and CD44^{+} populations cultured overnight without (upper graphs) or with cytokines (lower graphs); **D:** MFI of CD69, Granzyme B and IFN-γ expression by CD44^{-} (black bars) and CD44^{hi} (grey bars) GP33^{+} cells. Results are the mean+/SEM of 4 independent experiments. Differences determined using the Mann Whitney U-test were: ** $p \leq 0.01$, *** $p \leq 0.001$. **E:** Intra-cytoplasmic expression of INF-γ and Granzyme B by CD44^{-} (left) and CD44^{hi} CD8^{+} T cells (right) in one representative experiment.

Figure 4. The kinetics of GP33^{+} CD8^{+} T cells response to LCMV infection. C57BL/6 (B6) SPF mice were infected i.p. with 2x10^{5} PFU of LCMV Armstrong and studied at different time points after infection. **A:** Experimental protocol. **B:** Percentage of CD44^{hi}GP33^{+} cells in total GP33^{+} cells in spleen (SP) or bone marrow (BM) of SPF mice.**C:** Numbers of GP33^{+} CD8^{+} T cells recovered at each time-point after infection in spleen (SP) (black) and bone marrow (BM) (red). Differences determined using the Mann-Whitney U test were: *$p \leq 0.05$; ***$p \leq 0.005$. Significant different from SP at each time-point. **D, E:** BrdU incorporation by GP33^{+} cells during LCMV infection. Mice were injected i.p. with 1 mg/mouse of BrdU and

studied 1h after injection. Single-cell suspensions were obtained from inguinal (ING), brachial (BRA) and mesenteric lymph nodes (MES), SP and BM. Barriers defining $BrdU^+$ cells were determined in the same organs of control mice, which had not been injected with BrdU. **D:** Representative histograms of BrdU labelling by $CD44^{hi}GP33^+$ from different lymphoid organs of the same mouse at day 3 post-infection. **E:** The kinetics of BrdU incorporation in different organs, during LCMV infection. Each dot represents the percentage of $GP33^+BrdU^+$ cells found in the different organs from one individual mouse: **white dots:** $CD44^-GP33^+$ naïve cells in non-infected mice; **grey dots:** $CD44^{hi}GP33^+$ cells at day 3 after infection; **black dots** $CD44^{hi}GP33^+$ at day 5 after infection. Bars show the mean+/-SEM from 3-4 mice studied in two independent experiments. The difference between two groups was evaluated by the Mann-Whitney U test. Significant different from SP at each time-point. Single continuous variable data were analyzed by Kruskal-Wallis (KW) followed by Dunn's Multiple Comparison Test. The differences in BrdU incorporation: BM versus any other organ, at day 3: $p \leq 0.05$; at day 5: BM *vs* SP $p \leq 0.001$, BM *vs* MES $p \leq 0.01$; BM *vs* other organs $p \leq 0.05$.

Figure 5. The TRBV repertoire of $CD44^{hi}GP33^+$ cells is preferentially selected during LCMV infection. Results show the % of $GP33^+$ cells expressing TRBV13 (Vβ8) and TRBV29 (Vβ7) determined by the sequence of the TCRB chain of individual cells (A, C) or by staining with TCRB specific antibodies (B). (**A, B):** SPF mice: left: $CD44^-GP33^+$ cells (5 mice; 1.104 *tcrb* sequences), $CD44^{hi}GP33^+$ cells (3 mice; 250 *tcrb* sequences). (**B):** % of $GP33^+$ cells expressing Vβ8 or Vβ7 (mean+/-SEM of 3-5 mice studied in three independent experiments). (**C):** Black bars: $CD44^-GP33^+$ cells from SPF mice; Dashed bars: $CD44^{hi}GP33^+$ primary effector cells, at 7 days after infection (5 mice; 1097 *tcrb* sequences); white bars: memory cells 120 days after infection (4 mice; 795 *tcrb* sequences); and secondary effector

cells 7 days after infection (dashed bars) (white bars, 3 mice; 312 *tcrb* sequences). Differences by Kruskal-Wallis (KW) followed by Dunn's Multiple Comparison Test were: *$p \leq 0.05$, ** $p \leq 0.01$***$p \leq 0.001$.

Figure 6. **Microbiota stimulation imprinted CD44^{hi}GP33^{+}CD8^{+} T cells.** Results compared 12 weeks old SPF and GF mice, studied simultaneously. **A:** Numbers of CD44^{hi}CD8^{+} T cells recovered from the spleen (SP) and bone marrow (BM) of SPF (black bars) and GF (white bars) mice. Percentage (**B**) and total number (**C**) of CD44^{lo} and CD44^{hi} GP33^{+} cells recovered from the SP and the BM of SPF and GF mice. Each dot represents an individual mouse, and bars the SEM between different experiments. Representative histogram comparing the expression of CD49d in gated total CD44^{hi} CD8^{+} (**D**) and CD44^{hi} GP33^{+} cells (**E)** from SP of SPF and GF mice. The numbers in each histogram show the average percentage of positive cells from SPF (**upper numbers**) and GF **(lower numbers)** mice. **F:** Representative histogram comparing the expression of CD69 in gated BM CD44^{hi} CD8^{+} from SPF and GF mice. The numbers in each histogram show the average percentage of positive cells from SPF (**upper numbers**) and GF **(lower numbers)** mice. **G:** CD69 mean fluorescence intensity (MFI) on CD44^{-} (black bars) and CD44^{hi} GP33^{+} cells (grey bars) from SPF and GF mice. The numbers in each panel are the mean+/-SEM of 5-6 mice from each group, studied in three independent experiments. Differences evaluated using the Mann Whitney U-test were: *$p \leq$ 0.05; **$p \leq 0.01$; ***$p \leq 0.001$.

Figure 7. Microbiota with GP33 molecular mimicry generates CD44^{hi}GP33^{+} CD8^{+} T cells. A: Numbers of CD44^{hi}CD8^{+} T cells recovered from the spleen (SP) and bone marrow (BM) of SPF-1 (dark blue) and SPF-2 (light blue) mice. Percentage (**B**) and number (**C**) of CD44^{lo} and CD44^{hi} GP33^{+} cells recovered from the SP and the BM of SPF-1 (dark blue) and

SPF-2 (light blue) mice. Each dot represents an individual mouse, and bars the SEM between different experiments. **D:** Principal coordinate analysis (PCoA) of 16S RNA sequencing Operational Taxonomic Units (OTU) of the SPF-1 (dark blue) and SPF-2 (light blue) mice, along the first two principal coordinate (PC) axes based on Bray-Curtis distances and the respective PERMANOVA test. **E:** Relative abundance of some genus predicted to have cross-reactivity with GP33 peptide in the feces of SPF-1 (dark blue) and SPF-2 (light blue) mice. **H:** Volcano plot displaying differential microbiota genus between SPF-2 and SPF-1 mice. The vertical axis (y-axis) corresponds to the mean expression value of log 10 (q-value), and the horizontal axis (x-axis) displays the log 2 fold change value. The red dots represent the up-regulated genus in SPF-2 mice; the blue dots represent the genus downregulated in SPF-2 mice. Positive x-values represent up-regulation and negative x-values represent down-regulation. Fecal microbiota alpha diversity (**G**), calculated using the Shannon index (**H**), in SPF-1 (dark blue) and SPF-2 (light blue) mice. The numbers in each panel are the mean+/-SEM of 5 mice from each group, studied in two independent experiments. Differences evaluated using the Mann Whitney U-test were: $**p \leq 0.01$; $***p \leq 0.001$.

Figure 8. **Microbiota induce $CD44^{hi}GP33^{+}TRBV29^{+}$ IELs expansion in SPF mice. (A, B):** Results compared 12 weeks old SPF-1, SPF-2 and GF mice, studied simultaneously. **A:** IELs: representative dot plots. The upper panels show the gates used to select $CD69^{+}CD8\beta^{+}$IEL followed bellow by the identification of K^{b}-OVA-specific (Ova^{+}) and D^{b}-GP33-specific ($GP33^{+}$) IELs. The numbers in each panel are the mean+/-SEM (**upper numbers**) and % **(lower numbers)** of antigen-specific cells after acquisition of total IELs of 5-6 mice from each group, studied in three independent experiments. **B:** Numbers of $CD44^{hi}CD8^{+}$ T cells recovered from the IEL, lamina propria (LP) of SPF-1 (dark blue) SPF-2 (light blue) and GF mice (white). **(C):** Vβ7 expression by $GP33^{-}$ and $GP33^{+}$ IELs from 12 SPF-1 mice, studied in

three independent experiments. (**D)** The CDR3 a.a. composition of IELs from SPF-1 mice. Results correspond to CDR3 with 12 a.a. sequenced from 114 single-cells, from three mice studied in two independent experiments. The difference evaluated using the Mann Whitney U-test were: $^{**}p \leq 0.01$; $^{***}p \leq 0.001$.

A

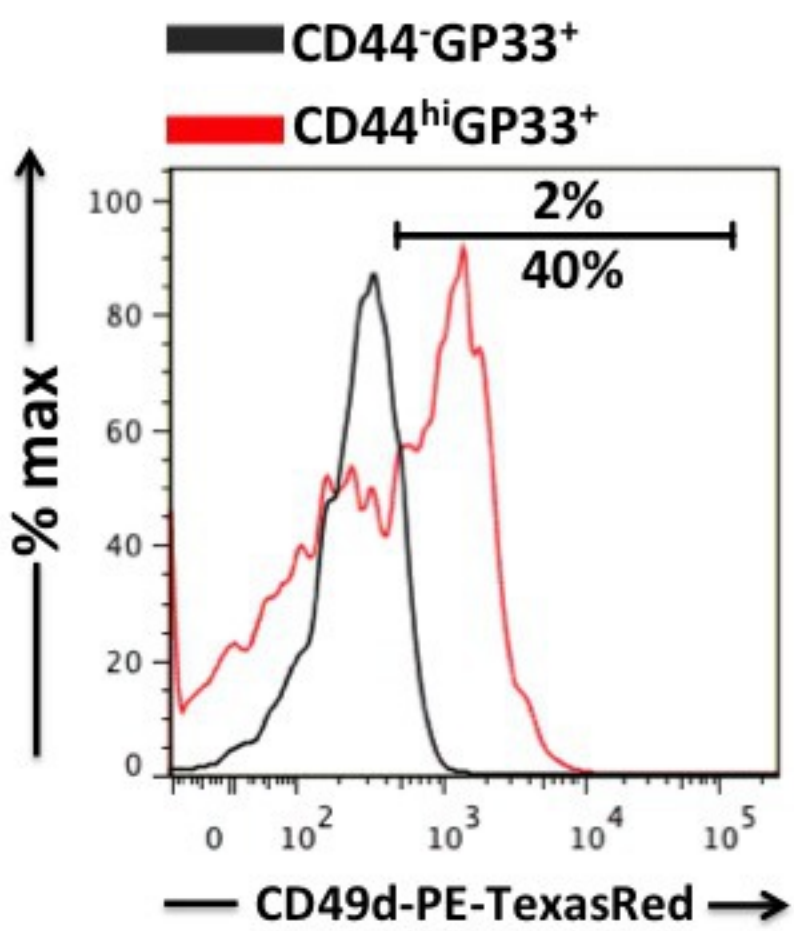
CD44-GP33+
CD44hiGP33+
2%
40%
% max
CD49d-PE-TexasRed

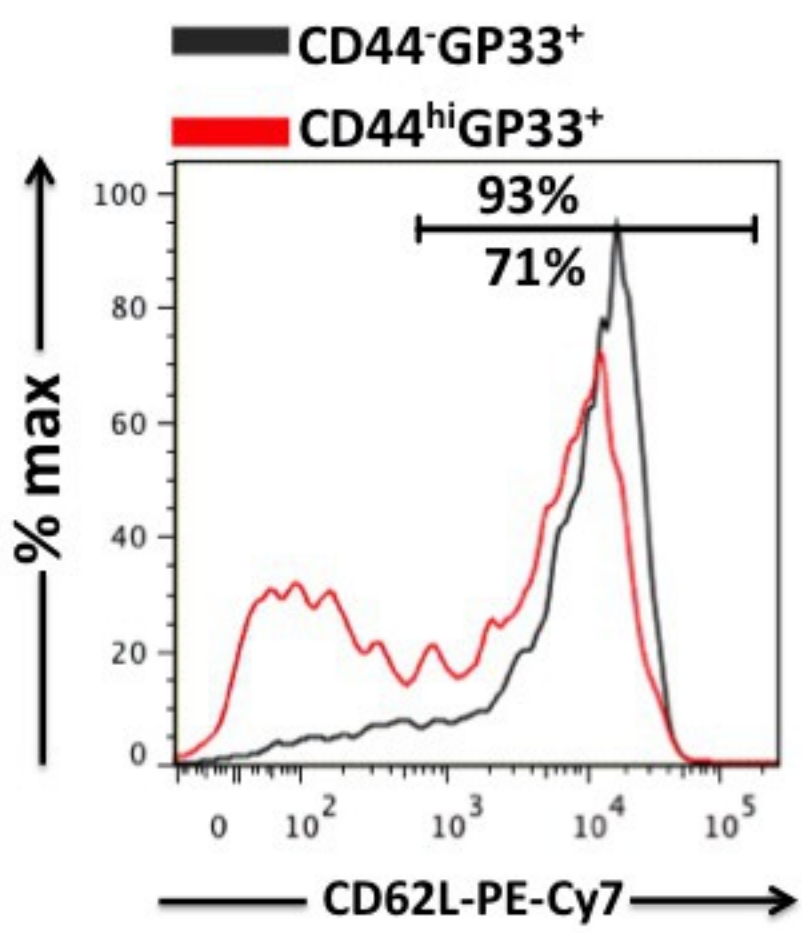
CD44-GP33+
CD44hiGP33+
93%
71%
% max
CD62L-PE-Cy7

B

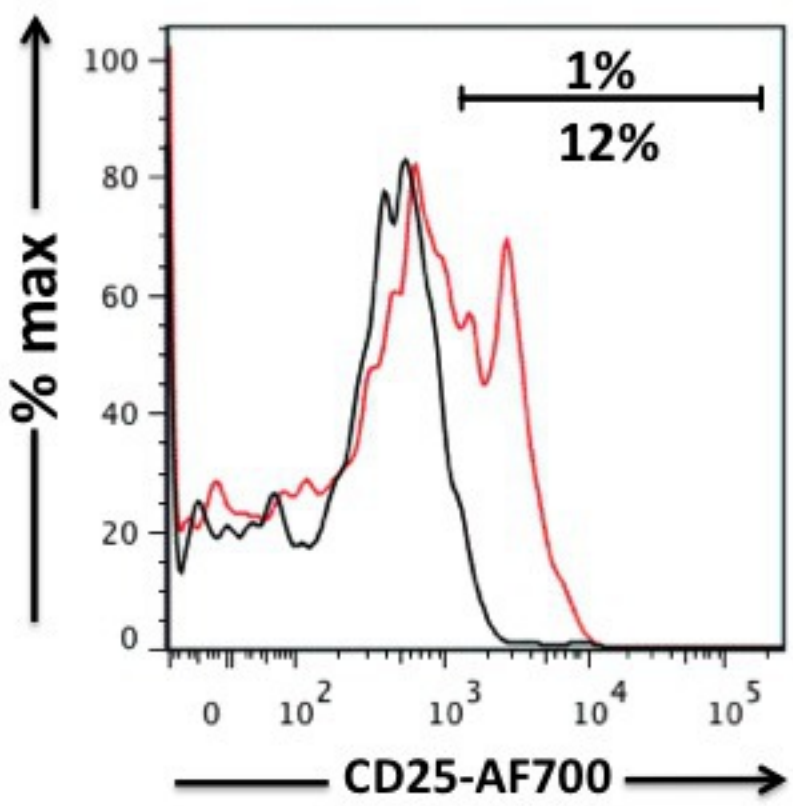
1%
12%
% max
CD25-AF700

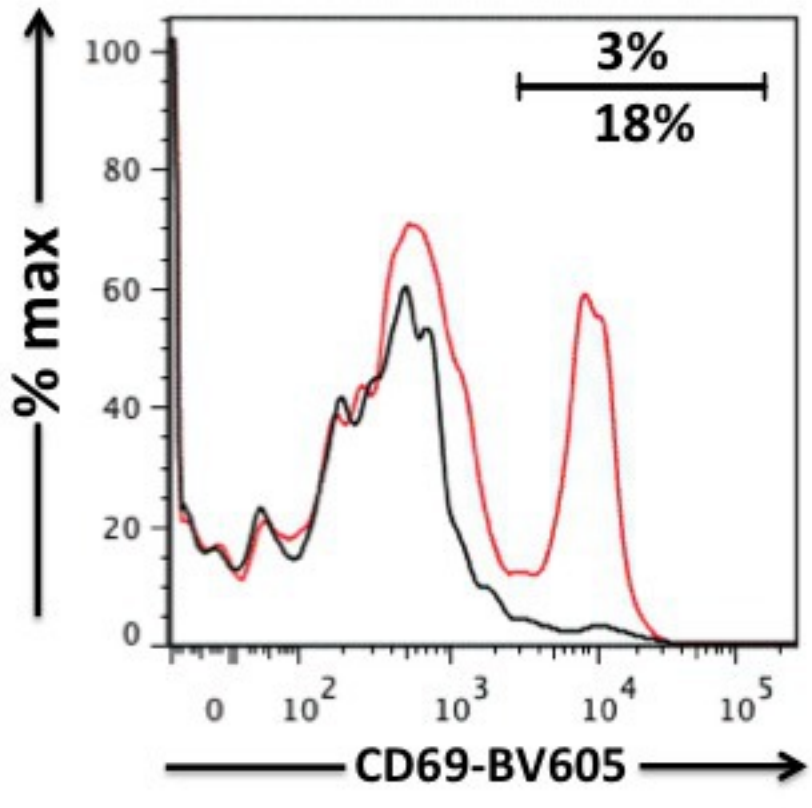
3%
18%
% max
CD69-BV605

C

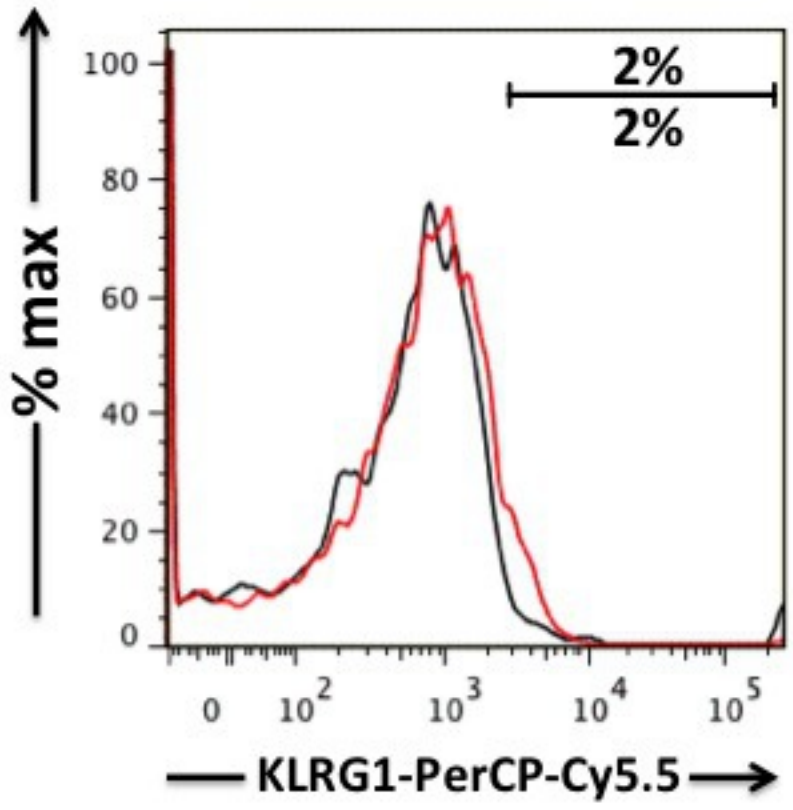
2%
2%
% max
KLRG1-PerCP-Cy5.5

D

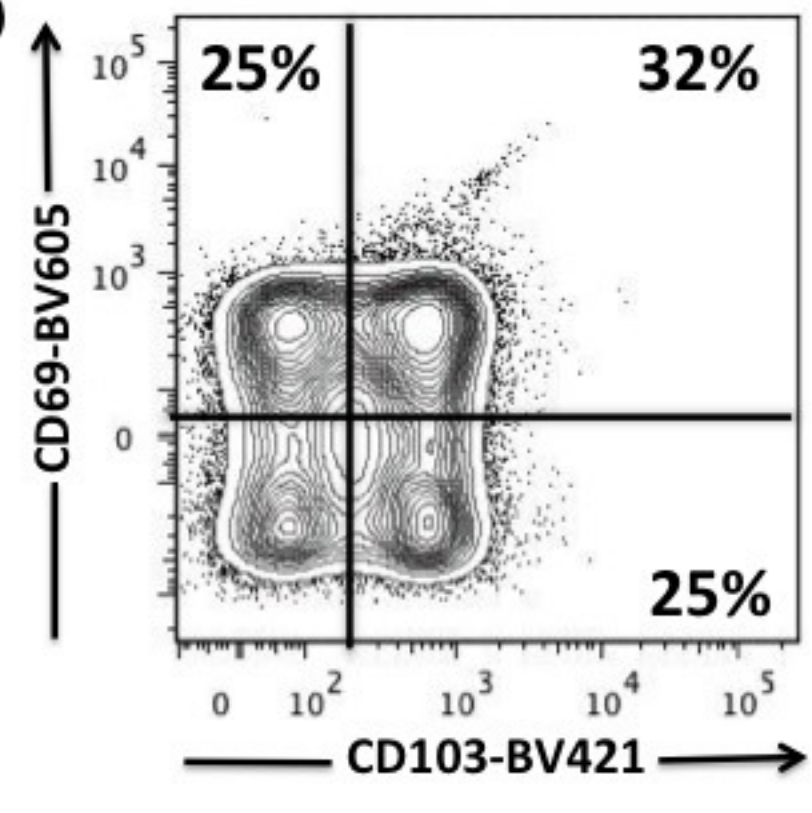
25%
32%
25%
CD69-BV605
CD103-BV421

E

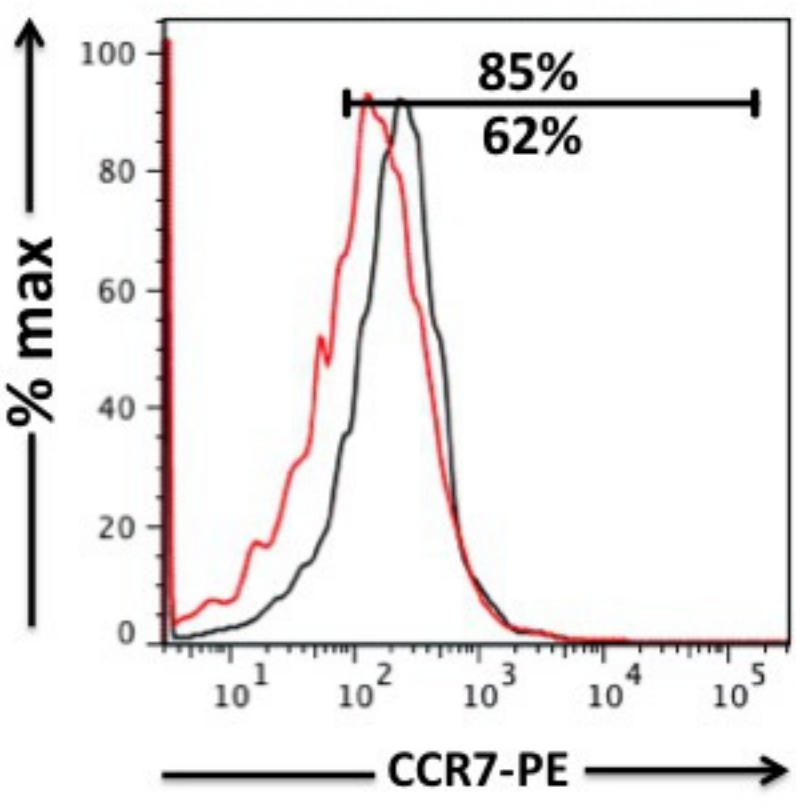
85%
62%
% max
CCR7-PE

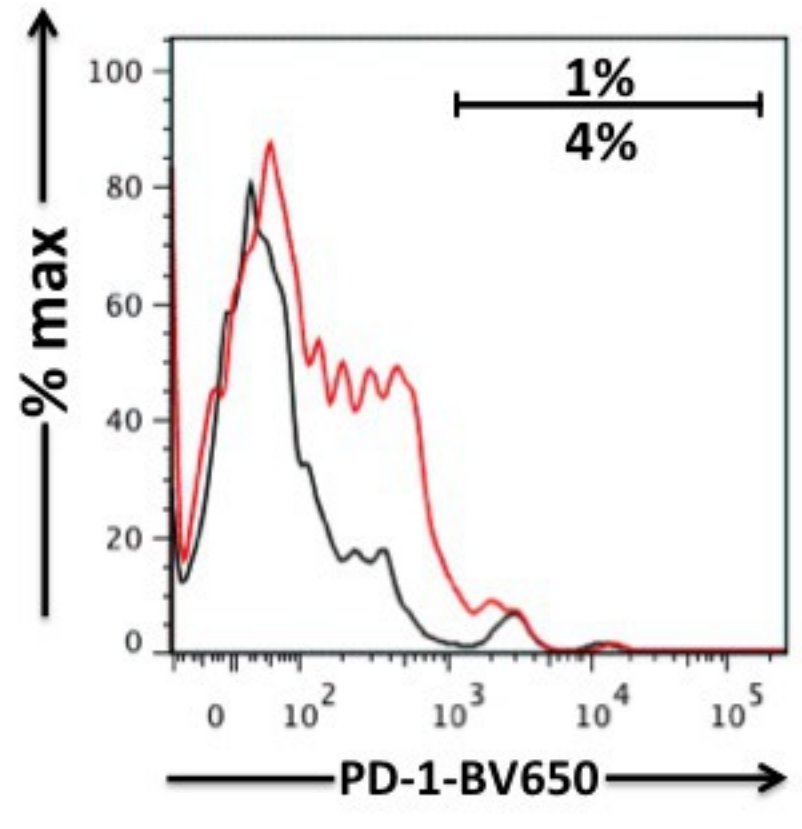
1%
4%
% max
PD-1-BV650

A

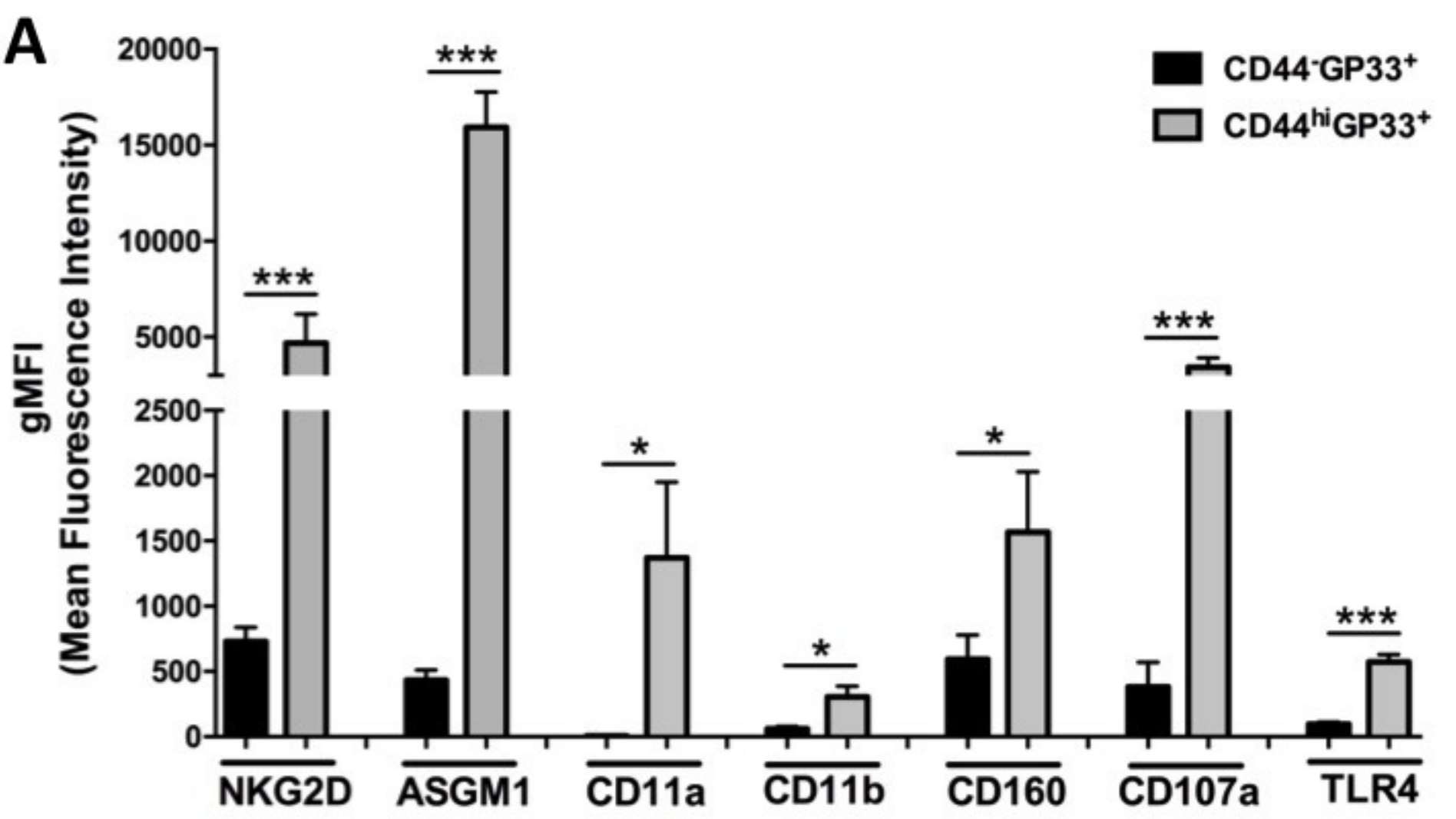
CD44-GP33+
CD44hiGP33+
gMFI
(Mean Fluorescence Intensity)
20000
15000
10000
5000
2500
2000
1500
1000
500
0
***
*
NKG2D
ASGM1
CD11a
CD11b
CD160
CD107a
TLR4

B

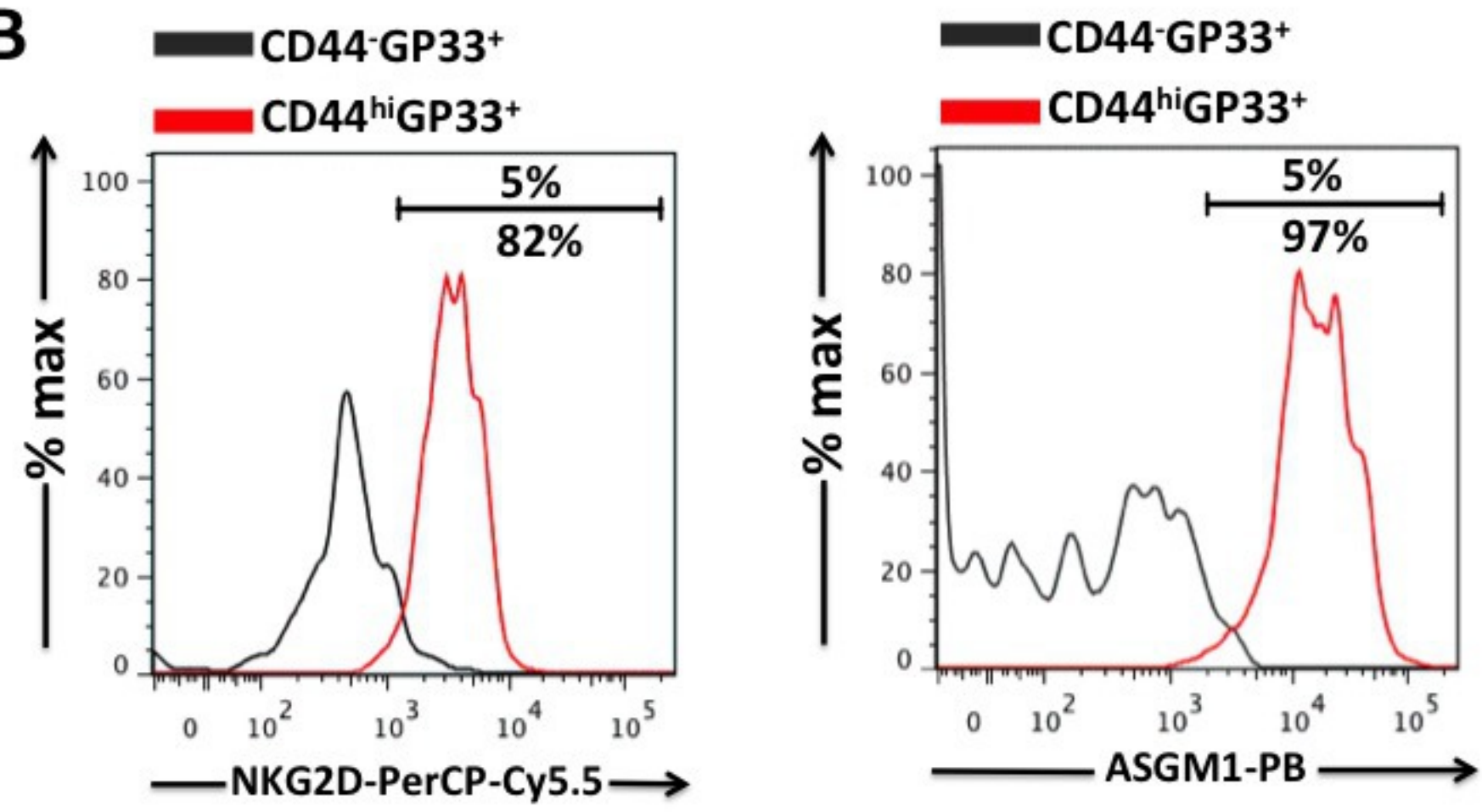
CD44-GP33+
CD44hiGP33+
% max
5%
82%
NKG2D-PerCP-Cy5.5
97%
ASGM1-PB
0%
57%
CD11a-PE
2%
13%
CD11b-AF700
4%
47%
CD160-PE-TexasRed
8%
37%
CD107a-FITC

C

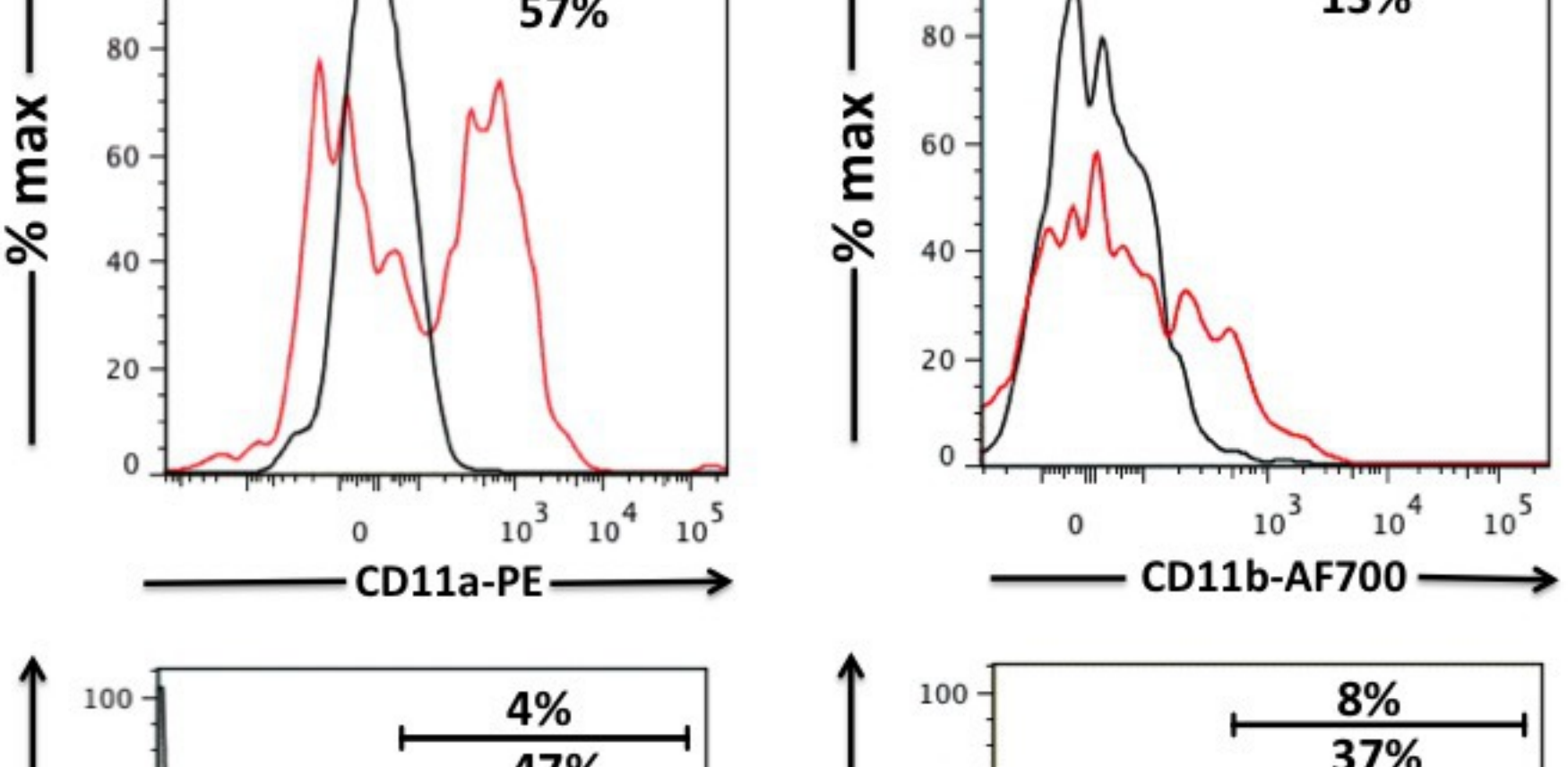
% max
0%
15%
CD284-PE-Cy7
CD44-APC-AF780
9%
CD284-PE-Cy7

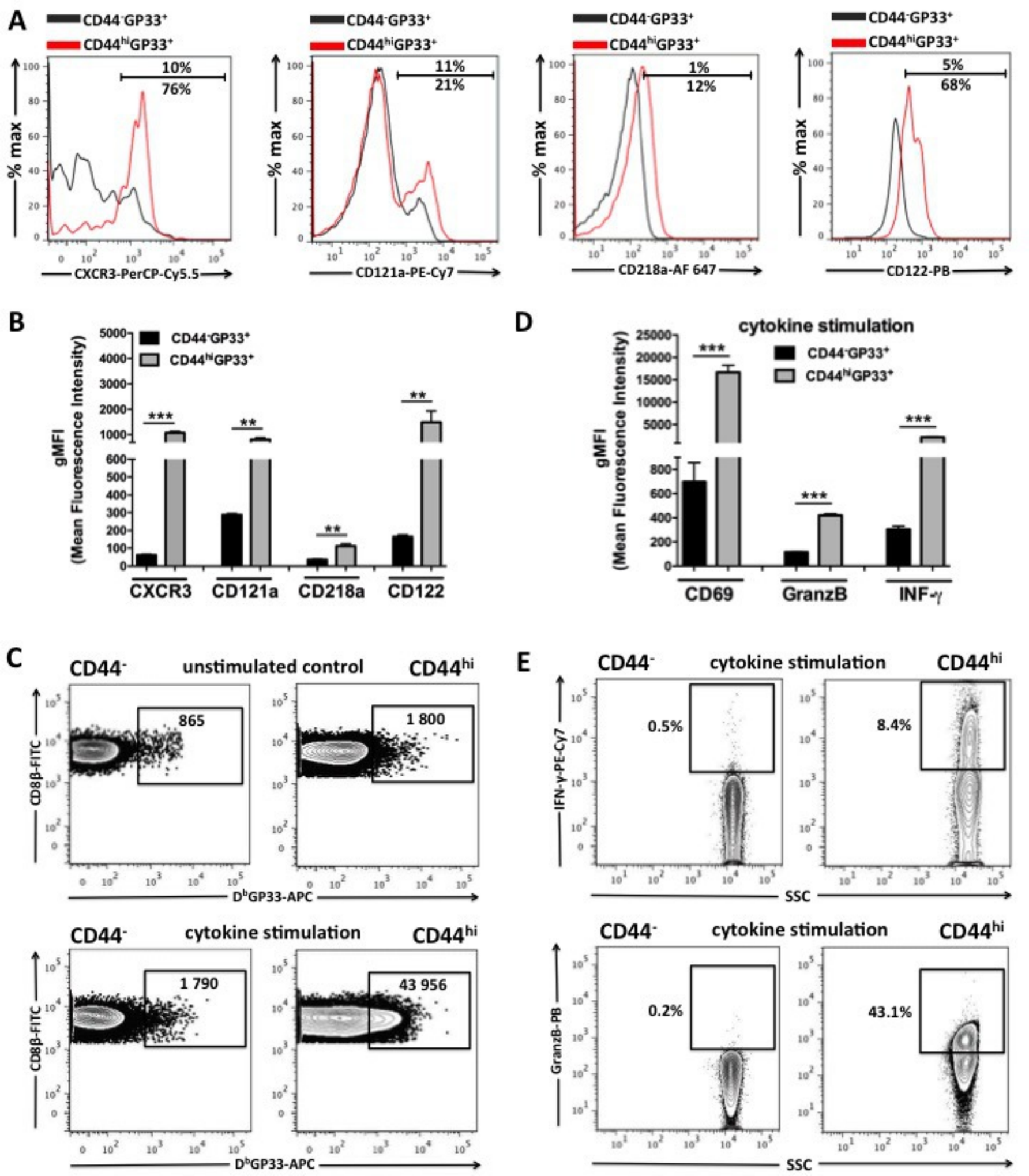
A
CD44-GP33+
CD44hiGP33+
10%
76%
11%
21%
1%
12%
5%
68%
% max
CXCR3-PerCP-Cy5.5
CD121a-PE-Cy7
CD218a-AF 647
CD122-PB
B
gMFI
(Mean Fluorescence Intensity)
CXCR3
CD121a
CD218a
CD122
D
cytokine stimulation
CD69
GranzB
INF-γ
C
CD44-
unstimulated control
CD44hi
865
1 800
CD8β-FITC
DbGP33-APC
cytokine stimulation
1 790
43 956
E
IFN-γ-PE-Cy7
0.5%
8.4%
SSC
GranzB-PB
0.2%
43.1%

A

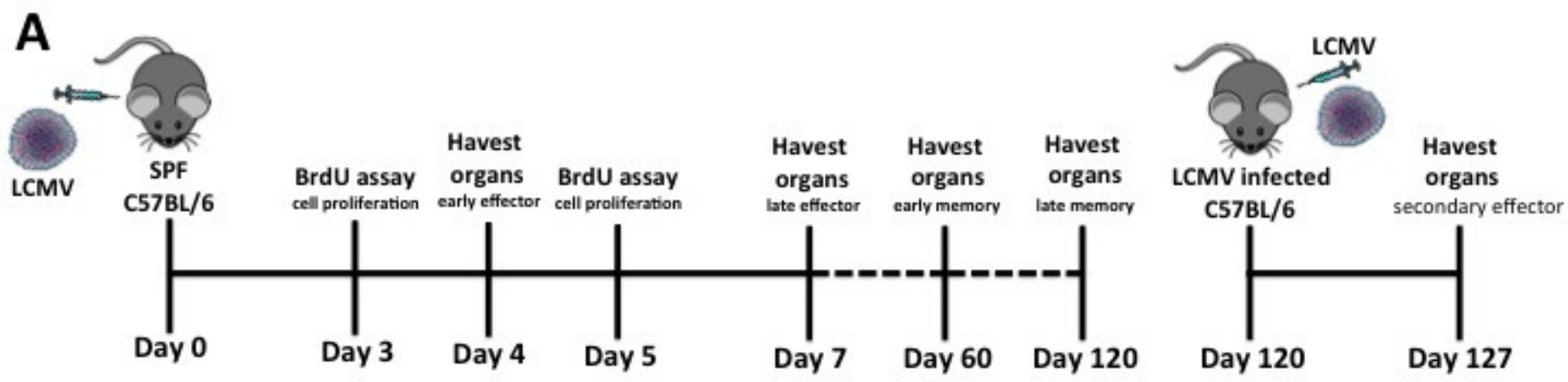
LCMV
SPF
C57BL/6
BrdU assay
cell proliferation
Havest
organs
early effector
BrdU assay
cell proliferation
Havest
organs
late effector
Havest
organs
early memory
Havest
organs
late memory
LCMV
LCMV infected
C57BL/6
Havest
organs
secondary effector
Day 0
Day 3
Day 4
Day 5
Day 7
Day 60
Day 120
Day 120
Day 127

B

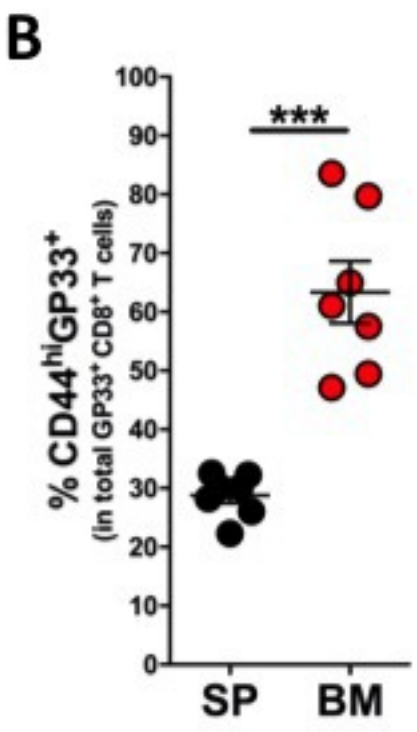
% CD44hiGP33+
(in total GP33+ CD8+ T cells)
***
SP
BM

C

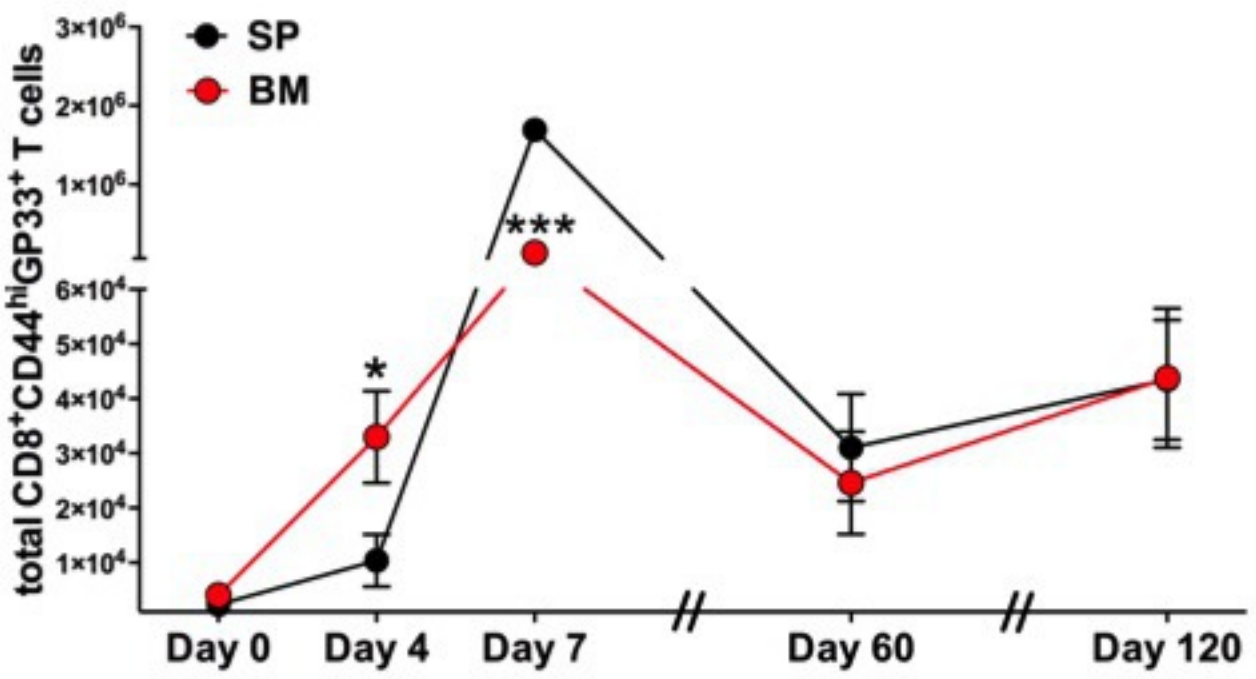
total CD8+CD44hiGP33+ T cells
SP
BM
*
***
Day 0
Day 4
Day 7
Day 60
Day 120

D

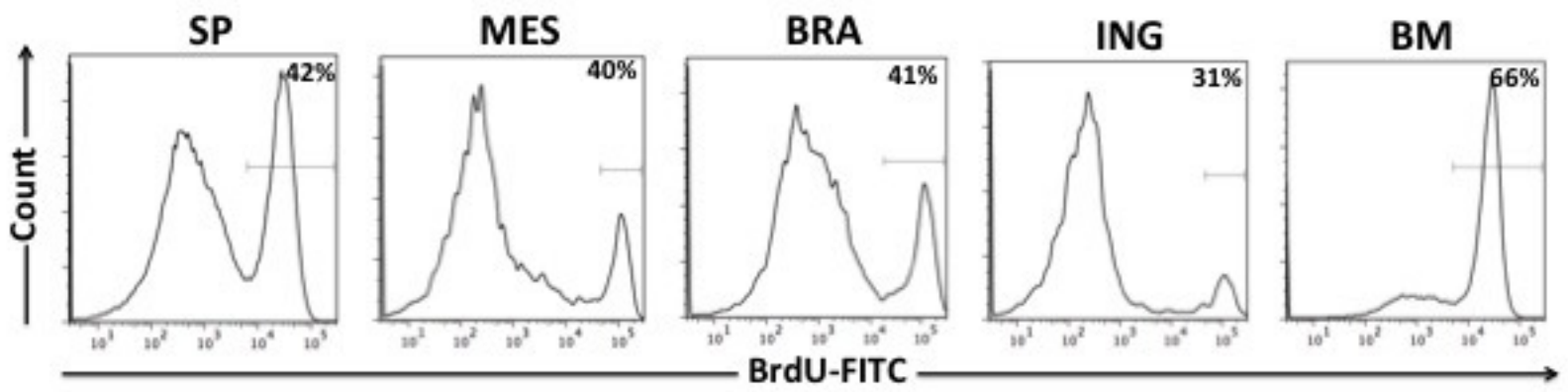
SP
MES
BRA
ING
BM
42%
40%
41%
31%
66%
Count
BrdU-FITC

E

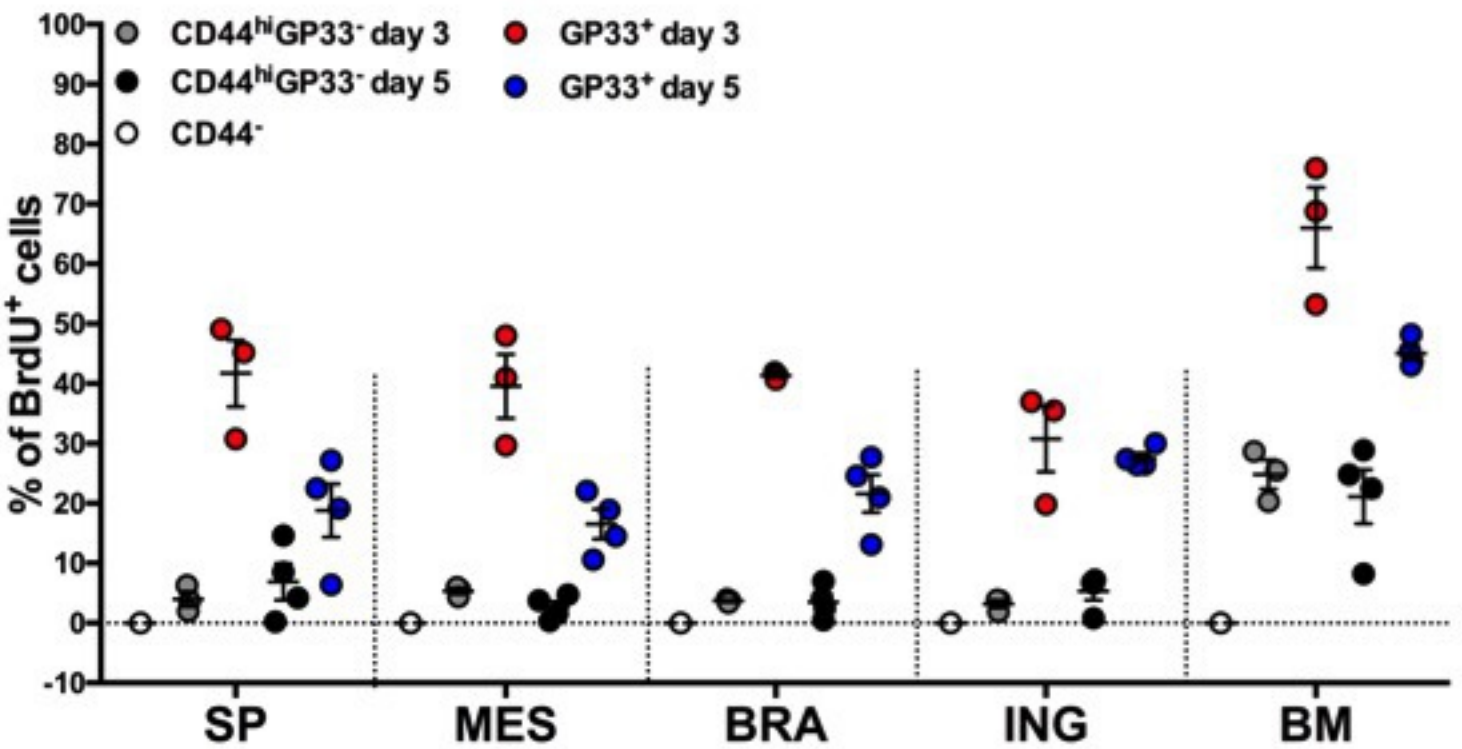
CD44hiGP33- day 3
CD44hiGP33- day 5
CD44-
GP33+ day 3
GP33+ day 5
% of BrdU+ cells
SP
MES
BRA
ING
BM

A

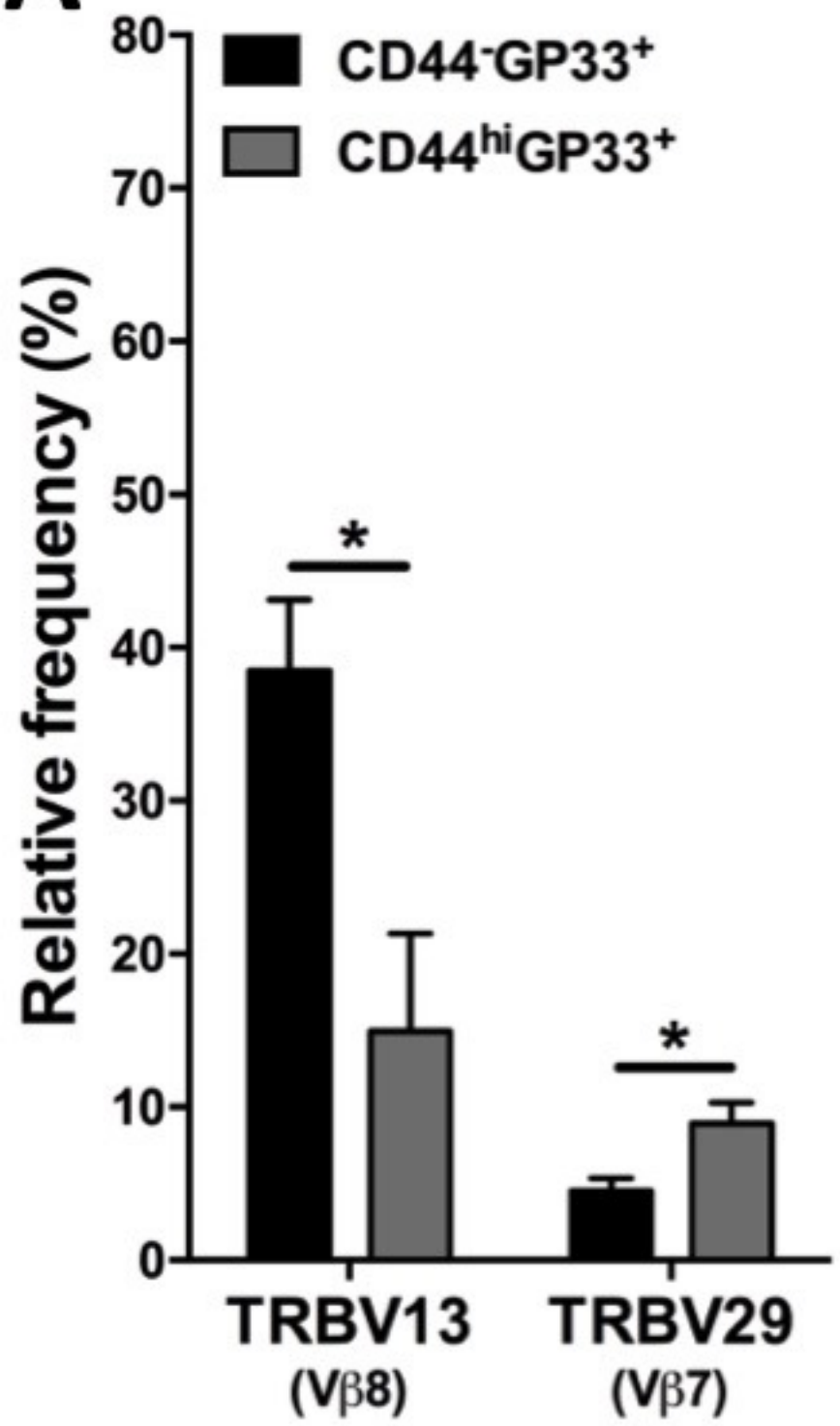
CD44-GP33+
CD44hiGP33+
Relative frequency (%)
80
70
60
50
40
30
20
10
0
*
*
TRBV13
(Vβ8)
TRBV29
(Vβ7)

B

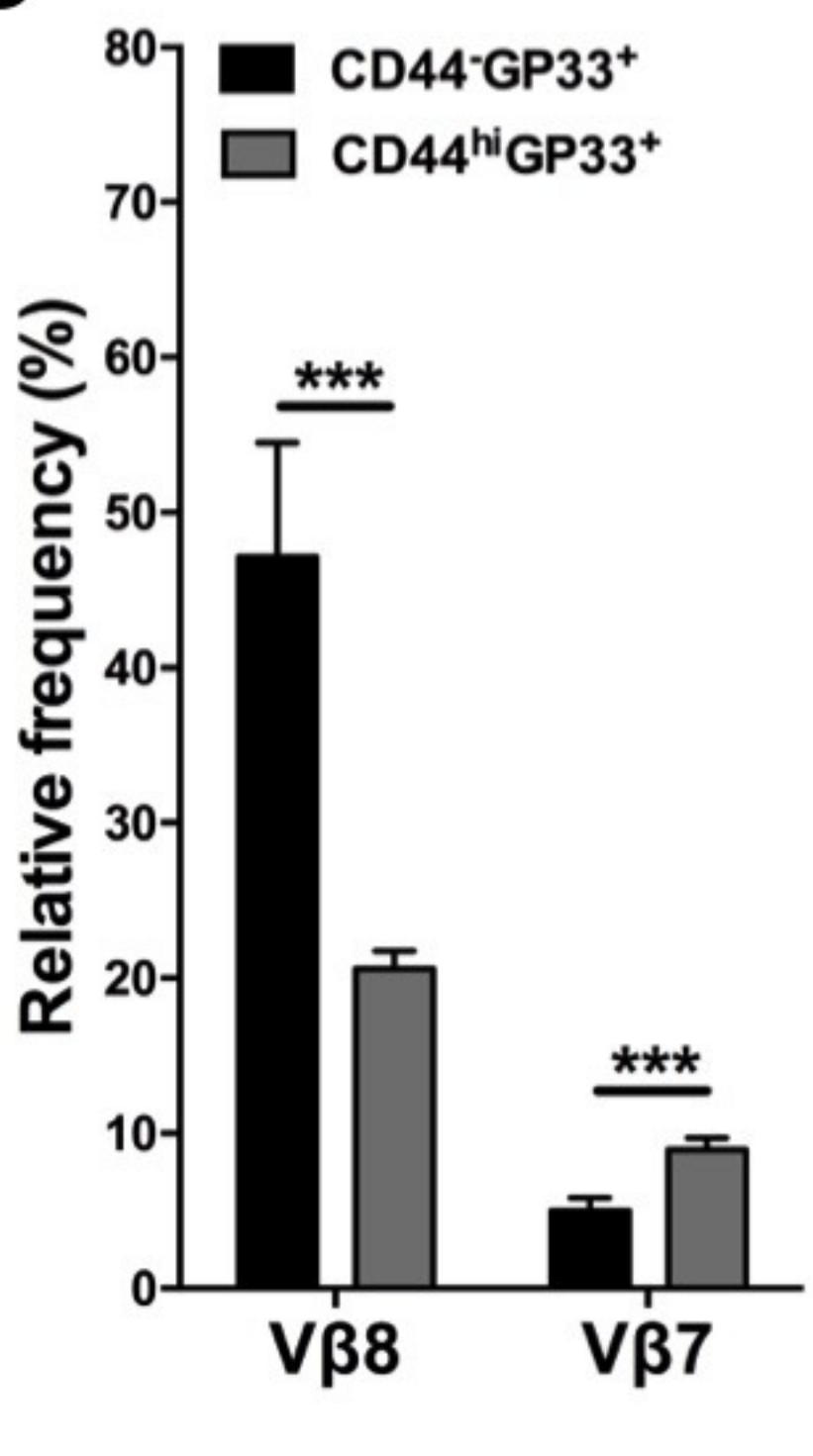
CD44-GP33+
CD44hiGP33+
Relative frequency (%)
80
70
60
50
40
30
20
10
0
***
***
Vβ8
Vβ7

C

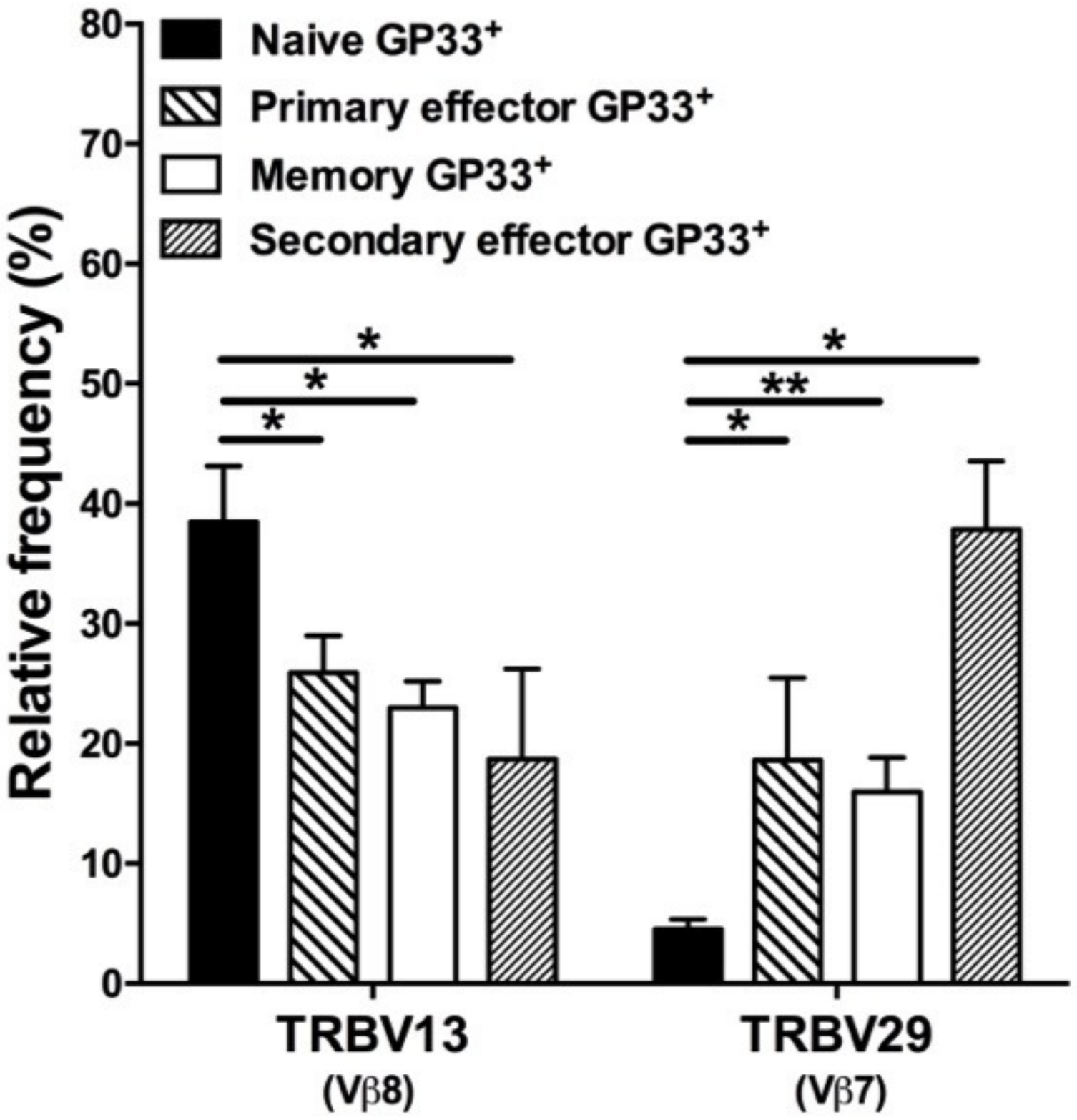
Naive GP33+
Primary effector GP33+
Memory GP33+
Secondary effector GP33+
Relative frequency (%)
80
70
60
50
40
30
20
10
0
*
*
*
*
**
*
TRBV13
(Vβ8)
TRBV29
(Vβ7)

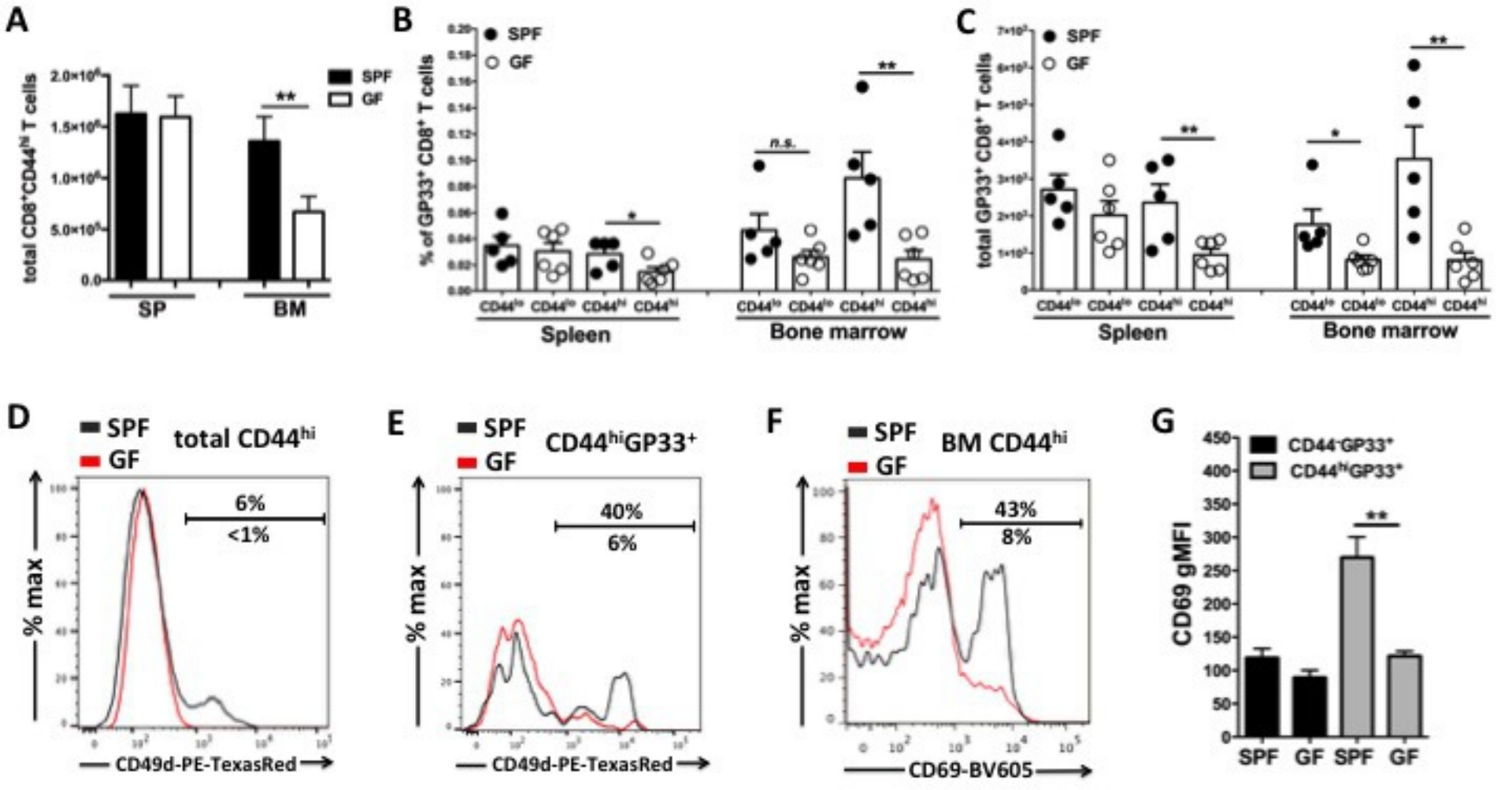
A
total CD8+CD44hi T cells
SPF
GF
**
SP
BM
B
% of GP33+ CD8+ T cells
SPF
GF
n.s.
*
**
CD44lo CD44lo CD44hi CD44hi
Spleen
Bone marrow
C
total GP33+ CD8+ T cells
SPF
GF
*
**
**
CD44lo CD44lo CD44hi CD44hi
Spleen
Bone marrow
D
SPF
GF
total CD44hi
6%
<1%
% max
CD49d-PE-TexasRed
E
SPF
GF
CD44hiGP33+
40%
6%
% max
CD49d-PE-TexasRed
F
SPF
GF
BM CD44hi
43%
8%
% max
CD69-BV605
G
CD44-GP33+
CD44hiGP33+
CD69 gMFI
**
SPF GF SPF GF

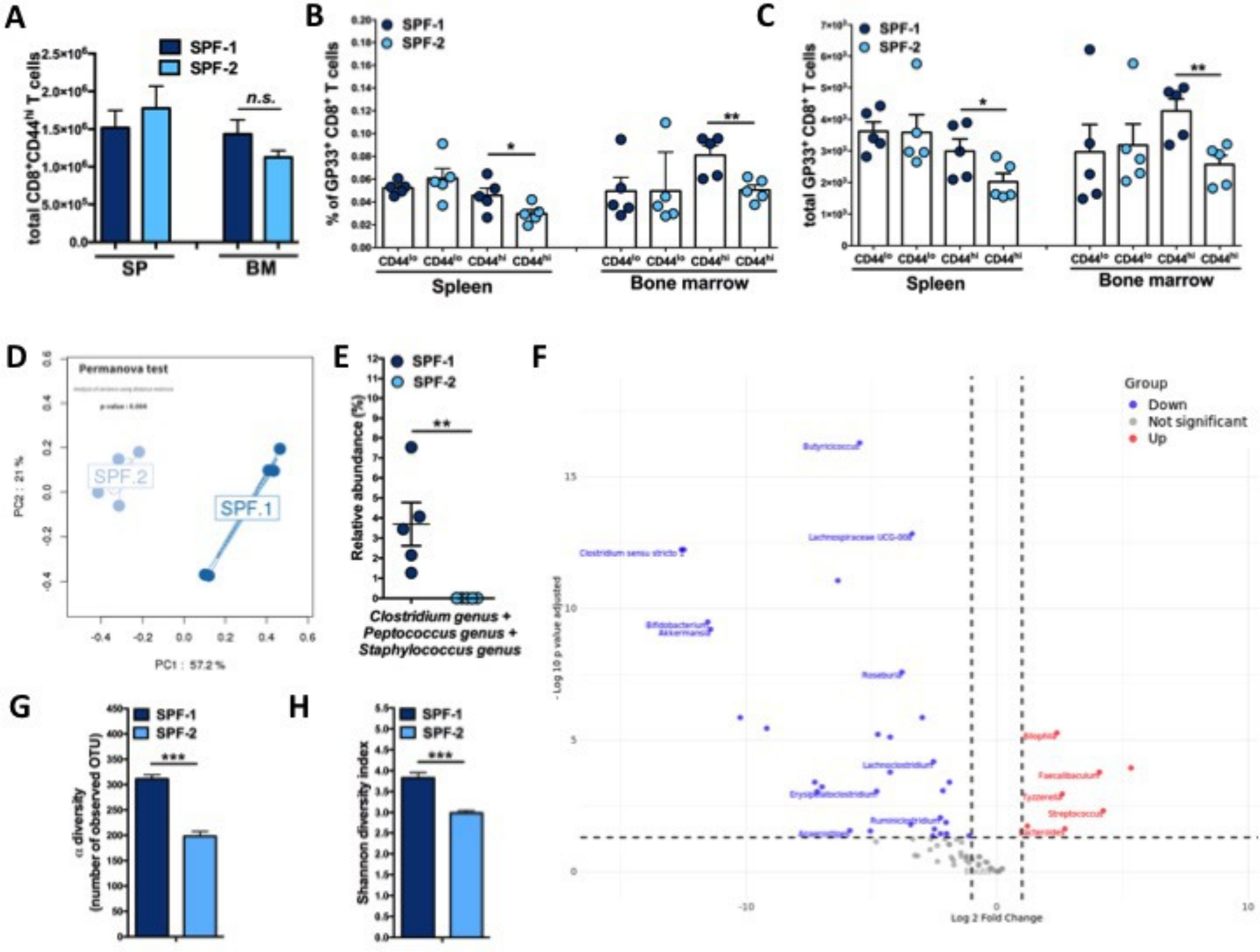
A
SPF-1
SPF-2
total CD8+CD44hi T cells
n.s.
SP
BM
B
SPF-1
SPF-2
% of GP33+ CD8+ T cells
CD44lo CD44lo CD44hi CD44hi
Spleen
Bone marrow
C
SPF-1
SPF-2
total GP33+ CD8+ T cells
CD44lo CD44lo CD44hi CD44hi
Spleen
Bone marrow
D
Permanova test
SPF.2
SPF.1
PC2 : 21 %
PC1 : 57.2 %
E
SPF-1
SPF-2
Relative abundance (%)
Clostridium genus +
Peptococcus genus +
Staphylococcus genus
F
Group
Down
Not significant
Up
- Log 10 p value adjusted
Log 2 Fold Change
Butyricicoccus
Lachnospiraceae UCG-006
Clostridium sensu stricto
Bifidobacterium
Akkermansia
Roseburia
Lachnoclostridium
Faecalibaculum
Streptococcus
Ruminiclostridium
G
SPF-1
SPF-2
α diversity
(number of observed OTU)
H
SPF-1
SPF-2
Shannon diversity index

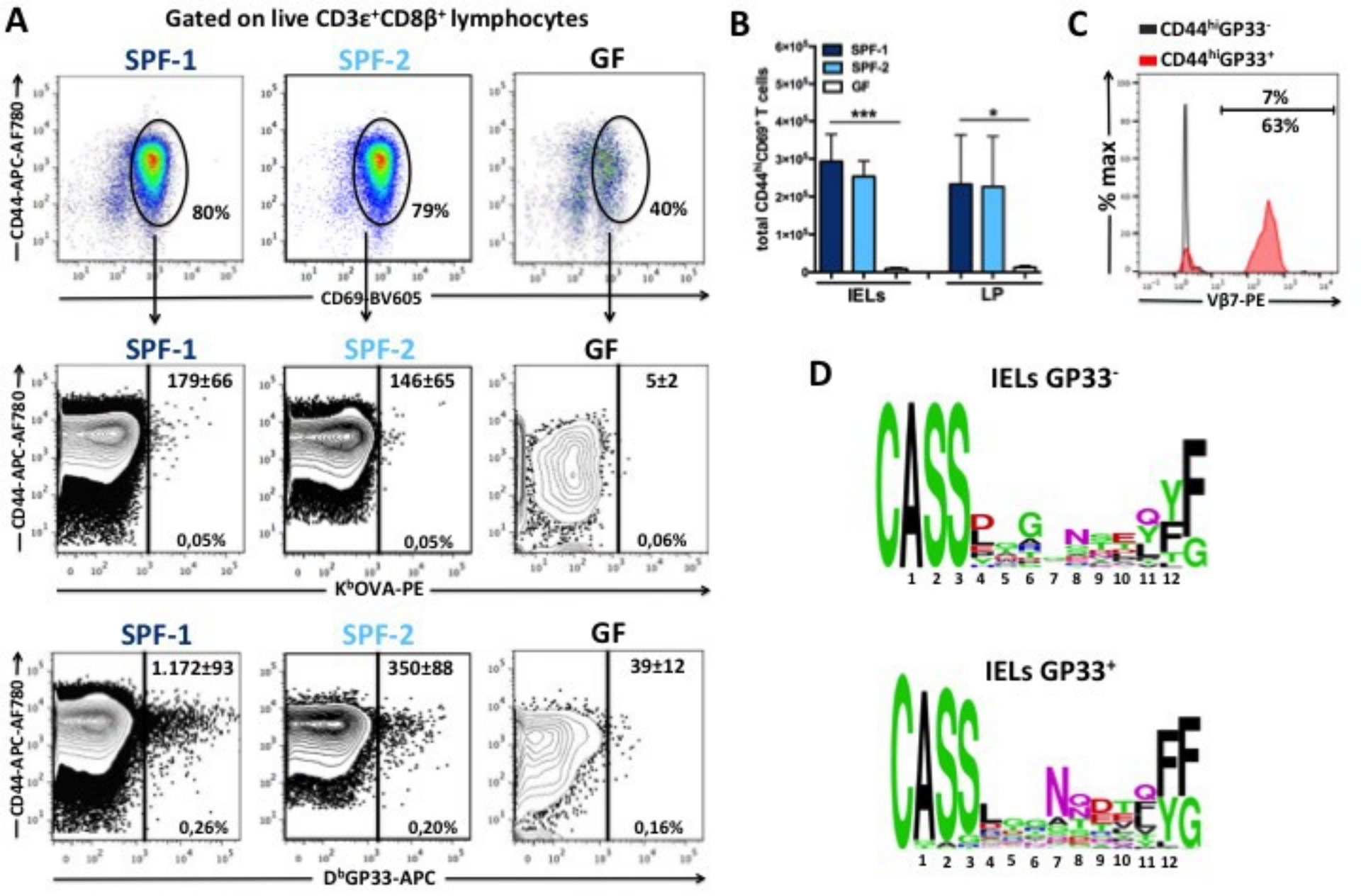
A
Gated on live CD3ε+CD8β+ lymphocytes
SPF-1
SPF-2
GF
CD44-APC-AF780
CD69-BV605
80%
79%
40%
K^bOVA-PE
179±66
146±65
5±2
0,05%
0,05%
0,06%
D^bGP33-APC
1.172±93
350±88
39±12
0,26%
0,20%
0,16%
B
total CD44^hiCD69+ T cells
SPF-1
SPF-2
GF
***
*
IELs
LP
C
CD44^hiGP33-
CD44^hiGP33+
% max
7%
63%
Vβ7-PE
D
IELs GP33-
IELs GP33+
1 2 3 4 5 6 7 8 9 10 11 12

Table 1. The diversity of GP33-specific $CD8^+$ T cells in primary effector phase, memory and secondary effector phase after LCMV infection.

CDR3β region	a.a.	TRBV	TRBJ	Total cells	Clones localized	Clones spread
Effector						
CASSFRDRGVAEQFF	13	4	2.1	3		x
CASSYSYEQYF	9	4	2.7	6	x	
CASSLDRGLEQYF	11	4	2.7	5		x
CASSSGTYNQAPLF	12	12.2	1.5	7	x	
CASSLGAGQLYF	10	12.2	2.2	8		x
CASSLWGTSAETLYF	13	12.2	2.3	2	x	
CASSDHTNTEVFF	11	13.1	1.1	3		x
CASSDNGNTEVFF	11	13.1	1.1	11		x
CASSDWTNTEVFF	11	13.3	1.1	8		x
CASSDWGNTEVFF	11	13.3	1.1	2	x	
CASSPGSYNSPLYF	12	16	1.6	2	x	
CASSLDGTSYAEQFF	13	16	2.1	13		x
CASSPWGAGEQYF	11	16	2.7	2		x
CASSLDDWGSYEQYF	13	16	2.7	3	x	
CASSPGTGGGYYAEQFF	15	17	2.1	2	x	
CATGTTNTEVFF	10	19	1.1	2	x	
CASSIQGNYAEQFF	12	19	2.1	2	x	
CASSIQGNYAEQFF	14	19	2.7	5		x
CASSLGGGDTEVFF	12	29	1.1	5	x	
CASSLWANSDYTF	11	29	1.1	13		x
CASSLVSNERLFF	11	29	1.4	22		x
CASSLWRGGAEQFF	12	29	2.1	5		x
CASSLFRDAEQFF	11	29	2.1	14		x
CASSLTPAEQFF	10	29	2.1	3	x	
CASSYWGSNTGQLYF	13	29	2.2	3		x
CASTPTSQNTLYF	11	29	2.4	5	x	
CASSLVTNQDTQYF	12	29	2.5	5	x	
CASSLTLNQDTQYF	12	29	2.5	13		x
CASSFTQGRDTQYF	12	29	2.5	3		x
CASSLGGAQDTQYF	12	29	2.5	12	x	
CASSLGGNQDTQYF	12	29	2.5	4	x	
CAWSLPGGNQDTQYF	13	31	2.5	22		x
CASSFRDRGVAEQFF	13	4	2.1	3		x
CASSYSYEQYF	9	4	2.7	6	x	
CASSLDRGLEQYF	11	4	2.7	5		x
Total clonotypes				**112**		
Total cells studied				**259**		
Sample size (x10^{-3})				**11.7**		
Memory						
CTCSAAGEGSQNTLYF	14	1	2.4	6		x
CASSQEDSISNERLFF	14	2	1.4	2		x
CASSMTGGAREQYF	12	3	2.7	2	x	
CASSPTDRGDTGQLYF	14	5	2.2	2	x	
CASSLGESQNTLYF	12	12.2	2.4	4		x
CASTTGGEEQYF	10	12.2	2.7	4		x
CASSPGAPFEQYF	10	12.2	2.7	2		x
CASSPWGYEQYF	10	12.2	2.7	2	x	
CASSDWTDTEVFF	11	13.1	1.1	3		x
CASSDAANTEVFF	11	13.1	1.1	3	x	
CASGDPIQYF	8	13.2	2.7	2		x
CASSDNSNTEVFF	11	13.3	1.1	4		x
CASSPGNSDYTF	10	13.3	1.2	4		x
CASSDAGGAREQYF	12	13.3	2.7	6		x
CARKGGGGEQYF	10	13.3	2.7	2	x	

CASSSGLGGLYAEQFF	14	15	2.1	3		**x**
CASSLLGVYEQYF	11	15	2.7	3	**x**	
CASSLDGGSYEQYF	12	16	2.7	10		**x**
CASSRARDNTEVFF	12	17	1.1	6		**x**
CASSYRGQQYF	9	17	2.7	2		**x**
CASSLGGGDTEVFF	12	29	1.1	2	**x**	
CASSLYPQDTQYF	12	29	2.5	4		**x**
CASSLGGNQDTQYF	12	29	2.5	9		**x**
CASSLSGDEQYF	10	29	2.7	3	**x**	
CASSLFRGYEQYF	11	29	2.7	2		**x**
CASSLLPGKYEQYF	12	29	2.7	2		**x**
Total clonotypes				**123**		
Total cells studied				**165**		
Sample size				**0.26**		
Secondary effector						
CASGDWGAYAEQFF	12	13.2	2.1	2	**x**	
CASSDAGGRDEQYF	12	13.3	2.1	2	**x**	
CASSFRDRGHAEQFF	13	14	2.1	2		**x**
CASSLRDRGHAEQFF	13	14	2.1	9		**x**
CASSPWDSNYAEQFF	13	14	2.1	16		**x**
CASSFWGTSAETLYF	13	15	2.3	2	**x**	
CASSRTEQDTQYF	11	15	2.5	4		**x**
CASSLDDWGSSYEQYF	14	16	2.7	2	**x**	
CGARGPQGNTEVFF	12	20	1.1	2		**x**
CGAREGNQAPLF	10	20	1.5	5	**x**	
CASSLFTNTEVFF	11	29	1.1	4	**x**	
CASSLSGGDTEVFF	11	29	1.1	2		**x**
CASSLSTGANSDYTF	11	29	1.2	9		**x**
CASSLSANTGQLYF	12	29	2.2	2		**x**
CASSLSLNTGQLYF	12	29	2.2	3	**x**	
CASSLFRDSAETLYF	13	29	2.3	3	**x**	
CASSWTGGSQNTLYF	13	29	2.4	8		**x**
CASSFSSQNTLYF	11	29	2.4	2	**x**	
CASSFGGNQDTQYF	12	29	2.5	6		**x**
CASSFVINQDTQYF	12	29	2.5	2		**x**
CASSLSRRVEQYF	11	29	2.7	5		**x**
Total clonotypes				**87**		
Total cells studied				**144**		
Sample size (x10^{-3})				**16.6**		

$CD8^+GP33^+$ cells from different LCMV infected mice were sorted from the SP, LN and BM to evaluate *Tcrb* expression in each individual cell from at different time points after LCMV infection. Results show a representative mouse at each time point. Remaining mice and full TCRB sequences of all individual cells in all mice are shown in Supplementary Table 2. From left to right: the CDR3 region; CDR3 size; *Trbv* gene; *Trbj* genes; the number of cells expressing the same TCRB, localized in a single organ (SP or LN or BM) (**localized**) or present in different organs (**spread**).

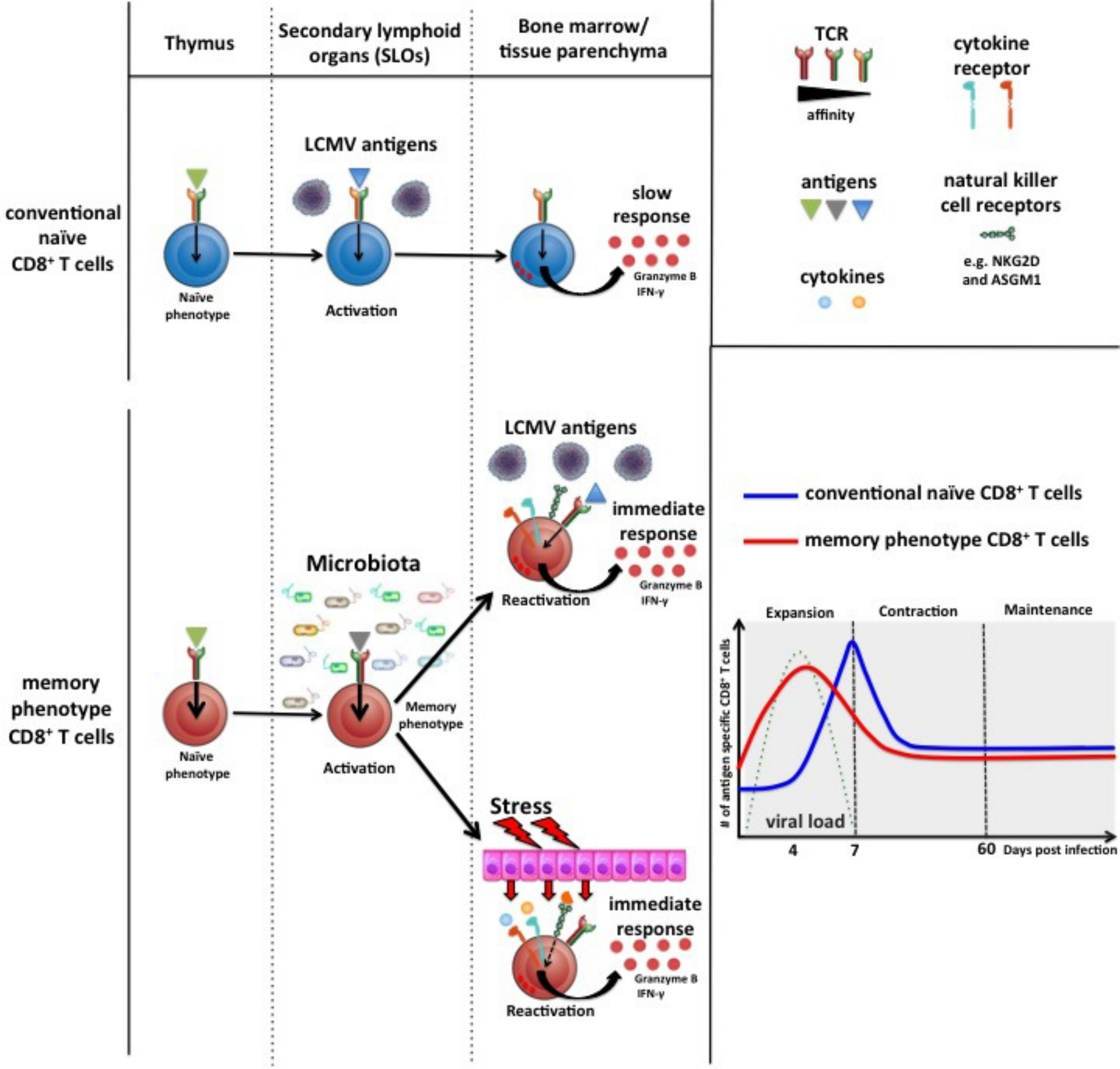
Thymus
Secondary lymphoid organs (SLOs)
Bone marrow/ tissue parenchyma
conventional naïve CD8+ T cells
LCMV antigens
Naïve phenotype
Activation
slow response
Granzyme B
IFN-γ
TCR
affinity
cytokine receptor
antigens
natural killer cell receptors
e.g. NKG2D and ASGM1
cytokines
memory phenotype CD8+ T cells
LCMV antigens
immediate response
Granzyme B
IFN-γ
Reactivation
Microbiota
Naïve phenotype
Activation
Memory phenotype
Stress
immediate response
Granzyme B
IFN-γ
Reactivation
conventional naïve CD8+ T cells
memory phenotype CD8+ T cells
Expansion
Contraction
Maintenance
# of antigen specific CD8+ T cells
viral load
4
7
60
Days post infection